Thesis for the degree of Doctor of Philosophy

Gyrokinetic simulations of turbulent transport in tokamak plasmas

Andreas Skyman

CHALMERS

Department of Earth and Space Sciences
CHALMERS UNIVERSITY OF TECHNOLOGY
Göteborg, Sweden 2014

Gyrokinetic simulations of turbulent transport in tokamak plasmas
ANDREAS SKYMAN
ISBN 978-91-7385-961-5

Doktorsavhandlingar vid Chalmers tekniska högskola
Ny serie nr. 3642
ISSN 0346-718X

Department of Earth and Space Sciences
Chalmers University of Technology
SE–412 96 Göteborg, Sweden
Phone: +46 (0)31–772 1000

Printed in Sweden
Chalmers Reproservice
Göteborg, Sweden 2014

Contact information:
Andreas Skyman
Department of Earth and Space Sciences
Chalmers University of Technology
Hörsalsvägen 9
SE–412 96i Göteborg, Sweden

Phone: +46 (0)31–772 1715
Fax: +46 (0)31–772 3663
Email: andreas.skyman@chalmers.se
URL: http://web.student.chalmers.se/~skymandr

Last updated on February 3, 2014.
An up to date version of this thesis will be available on the author's homepage.

Typeset in LaTeX using free open source software.

Gyrokinetic simulations of turbulent transport in tokamak plasmas

Andreas Skyman

Plasma Physics and Fusion Energy, Department of Earth and Space Sciences
Chalmers University of Technology

Thesis for the degree of Doctor of Philosophy

Abstract

With the enormous growth of high performance computing (HPC) over the last few decades, plasma physicists have gained access to a valuable instrument for investigating turbulent plasma behaviour. In this thesis, these tools are utilised for the study of particle transport in fusion devices of the tokamak variety.

The transport properties of impurities is a major part of the work. This is of high relevance for the performance and optimisation of magnetic fusion devices. For instance, the possible accumulation of He ash in the core of the reactor plasma will serve to dilute the fuel, thus lowering fusion power. Heavier impurity species, originating from the plasma-facing surfaces, may also accumulate in the core, and wall-impurities of relatively low density may lead to unacceptable energy losses in the form of radiation. In an operational power plant, such as the ITER device, both impurities of low and high charge numbers will be present.

This thesis studies turbulent particle transport driven by two different modes of drift wave turbulence: the trapped electron (TE) and ion temperature gradient (ITG) modes. Results for ITG mode driven impurity transport are also compared with experimental results from the Joint European Torus.

Principal focus is on the balance of convective and diffusive transport, as quantified by the stationary density gradient of zero flux ("peaking factor", PF). Quasi- and nonlinear results are obtained using the gyrokinetic code GENE, and compared with results from a computationally efficient multi-fluid model. The results are scalings of PF with the driving background gradients of temperature and density, and other parameters, including plasma shape and sheared toroidal rotation.

Keywords: fusion, plasma physics, tokamaks, gyrokinetics, turbulence, impurity transport, ITG, TEM, Joint European Torus, e-science

List of Appended Papers

This thesis is a summary of the following five papers. References to the papers will be made using roman numerals. In the list below, the author's contributions have been highlighted.

Paper I – H. Nordman, **A. Skyman**, P. Strand, C. Giroud, F. Jenko, F. Merz, V. Naulin, T. Tala and the JET-EFDA Contributors,
Fluid and gyrokinetic simulations of impurity transport at JET,
Plasma Physics and Controlled Fusion, vol. ***53***, no. 10, p. 105005
Contribution: gyrokinetic simulations and analysis thereof

Paper II – **A. Skyman**, H. Nordman, P. Strand,
Impurity transport in temperature gradient driven turbulence,
Physics of Plasmas, vol. ***19***, no. 3, p. 032313
Contribution: gyrokinetic simulations and analysis thereof; main author of the article, except section II.2

Paper III – **A. Skyman**, H. Nordman, P. I. Strand,
Particle transport in density gradient driven TE mode turbulence,
Nuclear Fusion, vol. ***52***, no. 11, p. 114015
Contribution: gyrokinetic simulations and analysis thereof; main author

Paper IV – **A. Skyman**, L. Fazendeiro, D. Tegnered, H. Nordman, J. Anderson, P. Strand,
Effects of the equilibrium model on impurity transport in tokamaks,
Nuclear Fusion, vol. ***54***, no. 1, p. 013009
Contribution: gyrokinetic simulations, except eigenvalue spectra, scaling with sheared toroidal rotation, and "full scenario"; main author in close collaboration with second author

Paper V – **A. Skyman**, H. Nordman,
Gyrokinetic modelling of stationary electron and impurity profiles in tokamaks,
Physics of Plasmas, (to be submitted)
Contribution: gyrokinetic simulations and analysis thereof; main author

Other contributions (not included)

This is a list of conference contributions and non-peer reviewed articles.

A – **A. Skyman**, H. Nordman, P. Strand, et al,
Impurity transport in ITG and TE mode dominated turbulence,
Proceedings of EPS 2010, Europhys. Conf. Abs., vol. 34A & poster, Dublin, Ireland
http://ocs.ciemat.es/EPS2010PAP/pdf/P1.1092.pdf

B – H. Nordman, **A. Skyman**, P. Strand, et al,
Modelling of impurity transport experiments at the Joint European Torus,
Proceedings of EPS 2010, Europhys. Conf. Abs., vol. 34A & poster, Dublin, Ireland
http://ocs.ciemat.es/EPS2010PAP/pdf/P1.1074.pdf

C – P. Strand, **A. Skyman**, H. Nordman,
Core transport studies in fusion devices,
SNIC progress report 08/09,
http://publications.lib.chalmers.se/records/fulltext/local_126485.pdf

D – P. Strand, **A. Skyman**, H. Nordman,
Core transport studies in fusion devices,
PDC 20th Anniversary & SNIC Interaction Conference 2010, (poster), Stockholm, Sweden
http://publications.lib.chalmers.se/records/fulltext/local_126486.pdf

E – **A. Skyman**, H. Nordman, P. Strand,
Turbulent impurity transport in fusion plasmas,
RUSA meeting 2010, (poster), Stockholm, Sweden
http://publications.lib.chalmers.se/records/fulltext/local_131418.pdf

F – **A. Skyman**, P. Strand, H. Nordman,
Turbulence and transport in multi ion species fusion plasmas,
PDC Newsletter, vol. 11, no. 1, p. 12,
http://www.pdc.kth.se/publications/pdc-newsletter/2011-1

G – **A. Skyman**, P. Strand, H. Nordman,
Turbulent impurity transport driven by temperature and density gradients,
13th International Workshop on H-mode Physics and Transport Barriers, (poster), Oxford, United Kingdom (2011)
http://publications.lib.chalmers.se/records/fulltext/local_147191.pdf

H – **A. Skyman**, H. Nordman, J. Anderson, et al ,
Turbulent particle transport driven by ion and electron modes,
Proceedings of EPS 2012, Europhys. Conf. Abs., vol. 36F & poster, Stockholm, Sweden
http://ocs.ciemat.es/EPSICPP2012PAP/pdf/P5.033.pdf

I – J. Anderson, H. Nordman, **A. Skyman**, R. Singh, P. Kaw,
High Frequency Geodesic Acoustic Modes in Electron Scale Turbulence,
Proceedings of EPS 2012, Europhys. Conf. Abs., vol. 36F & poster, Stockholm, Sweden
http://ocs.ciemat.es/epsicpp2012pap/pdf/P2.061.pdf

J – **A. Skyman**, J. Anderson, L. Fazendeiro, et al,
Particle transport in ion and electron scale turbulence,
Proceedings 24th IAEA FEC, article & poster, San Diego, USA (2012)
http://publications.lib.chalmers.se/records/fulltext/local_164285.pdf

K – J. Anderson, H. Nordman, **A. Skyman**, R. Singh, P. Kaw,
High Frequency Geodesic Acoustic Modes in Electron Scale Turbulence,
Proceedings 24th IAEA FEC, article & poster, San Diego, USA (2012)
http://publications.lib.chalmers.se/records/fulltext/local_165522.pdf

L – **A. Skyman**,
Transport of particles in electron and ion scale turbulence,
RUSA meeting 2012, (talk), Gothenburg, Sweden

M – **A. Skyman**, H. Nordman, P. Strand,
Turbulence, fusion and clean energy,
PDC Newsletter, vol. 14, no. 1, p. 4 *(main article)*,
http://www.pdc.kth.se/research/publications/pdc-newsletter/2013-1/

N – **A. Skyman**, L. Fazendeiro, D. Tegnered, et al,
Gyrokinetic simulations of turbulent transport in JET-like plasmas ,
Workshop on Impurity Transport, (talk), Gothenburg, Sweden (2013)

O – L. Fazendeiro, **A. Skyman**, D. Tegnered, et al,
Gyrokinetic simulations of turbulent transport in JET-like plasmas,
Proceedings of EPS 2013, Europhys. Conf. Abs., vol. 37D & poster, Espoo, Finland
http://ocs.ciemat.es/EPS2013PAP/pdf/P4.149.pdf

P – D. Tegnered, P. Strand, . . . , **A. Skyman**, et al,
Predictive simulations of impurity transport at JET,
Proceedings of EPS 2013, Europhys. Conf. Abs., vol. 37D & poster, Espoo, Finland
http://ocs.ciemat.es/EPS2013PAP/pdf/P4.137.pdf

Q – J. Anderson, H. Nordman, **A. Skyman**, R. Singh, P. Kaw,
High frequency geodesic acoustic modes in electron scale turbulence,
Nuclear Fusion, vol. 53, no. 12, p. 123016,
http://arxiv.org/pdf/1301.1435v2

Acknowledgements

First of all, let me thank my main supervisor, professor Hans Nordman, for his help and support. He has toiled bravely and cheerfully alongside me these last weeks, all the way to the crescendo. Cheers!

Second, John Johansson took the time to correct my grammar and to point out when literary ambition had won over clarity. Let it be known, that – his unpleasant visage and his frequent olfactory impositions on my person notwithstanding – he is a decent chap. I shall sorely miss your disruptive visits!

Third, some credit is long overdue for Lady Ada Lovelace and Dr Grace Hopper, without whose groundbreaking work none of this would be possible.

Finally, my friends: you are the world to me.

Credits & About

This thesis was written in LaTeX, using latex templates made by Markus Billeter and Ludde Edgren.

Billeter's template was originally created by Fredrik Warg and updated by Martin Thuresson. The template will be made available at

http://www.cse.chalmers.se/~billeter

This document uses images from the 'Silk Icons Set 1.3' by Mark James. These are licensed under a Creative Commons Attribution 2.5 License and available at http://www.famfamfam.com/lab/icons/silk/.

The document also uses 'ccBeamer 0.1' by Sebastian Pipping, which is licensed under Creative Commons Attribution–ShareAlike 3.0, available at

http://blog.hartwork.org/?p=52

In compliance with the Swedish Research Council's policy on Open Access, the whole thesis is licensed under the Creative Commons Attribution-ShareAlike 3.0 License. For details on the licenses, see page ii. To learn more about Open Access, go to

http://www.openaccess.se

An up to date version of this thesis will be available on the author's homepage.

Long live ☺! :wq

Table of contents

Part I

Summary

"It always takes twice as long as you think. Even if you double your estimate. Something of a natural law."

Mr J. J. Tobias [1]

1

Introduction

1.1 Nuclear fusion

In a conventional nuclear power plant, the fuel consists of heavy elements whose nuclei split and form lighter atoms, in what is known as fission. Fusion, on the other hand, is the nuclear process where two lighter nuclei combine to form a heavier element. This does not happen naturally on Earth, but elsewhere in the universe it is commonplace: it is fusion that powers the stars. This was realised around the 1920s by Sir Arthur Eddington, and the dream of utilising this process for energy production was kindled at the same time [2].

Though fusion and fission power require very different operating scenarios, the fundamental principle that allows both fusion and fission to occur and release energy is the same. As can be seen in figure 1.1, the mass of an atom is not simply the sum of its nucleons – its neutrons and protons. This phenomenon is called the *mass defect*. [3] As neutrons and protons are added to or subtracted from an element, the combined mass is decreased if the product is closer to the minimum in the figure. The most common isotope of iron, ^{56}Fe, has been highlighted ($\square$) in the figure. As can be seen, iron is at the minimum of the mass curve, meaning that it is the element with the least mass per nucleon.

By Einstein's relation $E = mc^2$ [4] mass is a form of energy, wherefore the decrease in mass is also a decrease in energy, and generally, decreased energy means increased stability. The tendency of elements combining or falling apart to form more "iron like" elements is spontaneous, in the sense that it is statistically more likely to occur than the opposite. This can be understood from figure 1.1, by observing that in order to bring an element away from the minimum, mass in the form of energy has to be supplied from somewhere. The conservation of energy – one of the most fundamental principles in all of Physics – demands that the missing mass be turned into other forms of energy, and it is this energy that is captured in nuclear power plants of both varieties. The typical fuel for fusion and fission are represented in figure 1.1 by the two highlighted isotopes ^{2}H and ^{238}U (Uranium) respectively. The ^{2}H is the isotope of Hydrogen called "heavy Hydrogen", which is more commonly known as Deuterium and denoted D in plasma physics. As can be seen, the energy that can potentially be gained by fusing light elements is many times greater per nucleon, and hence per kilogramme of fuel, than that which fission yields.[1] This is one of the reasons why fusion as a power source is so attractive.

That the fusion process is essentially spontaneous does not mean, however, that it is easy to accomplish. Whereas fission happens spontaneously on Earth, fusion requires much more exotic circumstances. In fission power plants, the nuclear process is mediated by neutrons, whereas for fusion to occur, the electrostatic repulsion between the positively charged nuclei needs to be overcome. Methods of accomplishing this normally require either extreme temperatures, extreme pressure, or a combination of the two. At sufficiently high temperature, collisions between atoms will be energetic enough to separate the electrons from the nuclei, creating ions. If the frequency of recombining collisions is sufficiently low compared to the frequency of ionising collisions, a plasma is the result [6], meaning that it is easier to ionise a thin gas than a dense one. For fusion to occur, however, the resulting ions need to collide with enough force, that they break through the repulsive potential of the nuclear charges. The probability of a nuclear reaction to occur is quantified by the *cross section* for the reaction. The most favourable cross section for fusion is obtained for the fusion between Deuterium and Tritium (^{3}H) in the reaction [3, 6]:

$$\mathrm{D} + \mathrm{T} \equiv {}^{2}\mathrm{H} + {}^{3}\mathrm{H} \longrightarrow {}^{4}\mathrm{He} + \mathrm{n} + 17.6\,\mathrm{MeV} \tag{1.1}$$

where ^{4}He is an ordinary Helium ion, more often referred to as an α-particle, and n is a neutron. The total excess energy from the reaction in equation (1.1) is 17.6 MeV, distributed on the fusion products according to their mass, so that the total momentum is conserved, meaning that $\sim 4/5$ of the energy is deposited on the neutron. Because the neutron is uncharged, it is not confined by the magnetic fields used to contain the plasma, and will therefore leave the core region, depositing it energy in the wall of the plasma chamber, which is how energy will be extracted in a working power plant. The α-particles, on the other hand, will be caught in the magnetic field and, through collisions, deposit their excess energy to the fuel ions, heating the plasma. Efficient α-particle heating is a key component in achieving self-sustained nuclear fusion. Unfortunately, Tritium is not a stable isotope of Hydrogen. It is radioactive with a half-life of

[1] The scale in figure 1.1 is in eV, or *electron Volts*. $1\,\mathrm{eV} \approx 1.6 \cdot 10^{-19}$ J, meaning that you would need roughly $2.5 \cdot 10^{19}$ eV to heat 1 g of water 1 °C, but considering that Deuterium atoms are $\sim 1.5 \cdot 10^{26}$ to a kilo, there is still a lot of energy in one nuclear reaction [5].

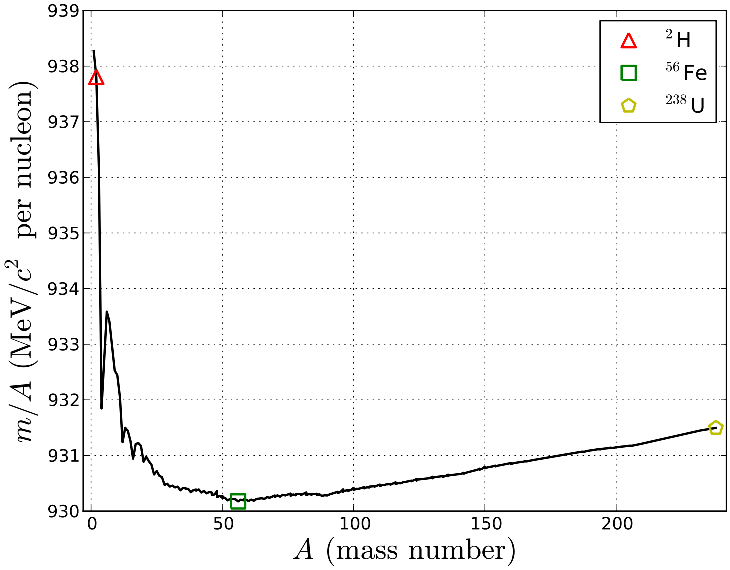

Figure 1.1: *Mass defect for the stable nuclei. Deuterium (^{2}H; △) and Uranium (^{238}U; ⬠) are indicated. Spontaneous fusion and fission moves towards the energy minimum (^{56}Fe; □). Based on data from [9] and [3].*

12.33 years, and so must be manufactured. This can for instance be by *breeding* from Lithium, an element that is abundant in the Earth's crust [3, 5, 7, 8].

A striking example of fusion in Nature is the sun, which relies on the force of gravity to create the immense pressure needed for the fusion of protons and other elements to occur, which is the process that makes it and all other stars shine. The circumstances under which fusion can take place are very exotic from an Earthly stand-point, and very difficult to produce in a laboratory. Creating the conditions of allow for a high enough fusion cross section requires highly specialised devices and knowledge, which is why the engineering and science aspects of fusion research are both very important.

1.2 Fusion plasmas

1.2.1 The fourth state of matter

Super-heating or sufficiently depressurising a gas will eventually, through the processes outlined in section 1.1, lead to the separation of the electrons from the atoms in the material, resulting in an ionised gas – a plasma. In analogy with the solid, liquid and gaseous states of matter, plasmas are often referred to as the *fourth state* of matter.

A more rigorous definition of a plasma is that

> *"[a] plasma is a quasineutral gas of charged and neutral particles which exhibits collective behaviour"* [6],

where quasineutral means that the plasma is electrically neutral when viewed from a distance, but may exhibit charge fluctuations on small scales. In many ways a fluid,[2] plasmas are subject to the already complicated laws of fluid mechanics, but their behaviour becomes even more embroiled by the electromagnetic properties of the plasma, which introduce long range effects not present in other media. These effects are what lead to collective behaviour in the plasma, and this property is the most important difference between a partly ionised gas and a proper plasma. The intermingling of these two areas of physics further implies, that acoustic and electromagnetic waves coexist in the plasma, but often on very different time and length scales. This makes both analytical and numerical studies of the governing equations very challenging, if one wishes to capture the entirety of this intricate interplay.

Though exotic in many ways, plasmas exist in our everyday surroundings: in fluorescent tubes, neon signs and modern television sets. The kind of plasmas that occur naturally on Earth are rarer, but not uncommon. The Northern[3] lights and lightning are perhaps the most well known examples. Fusion plasmas, however, need to be much hotter in order to have a high enough fusion cross section for fusion power to be feasible. In order to sustain a fusion grade plasma in a laboratory or a reactor, it needs to be separated from the surroundings; it needs to be confined.

In the sun and the stars, the confinement is accomplished by gravity, where the mass of the stellar body is enough to create the pressure needed for the fusion process to be self sustained. This is not, however, an option for earthbound plasmas.[4] Instead, research into confining plasmas is divided into two main areas: magnetic and inertial confinement. The first method is the topic of this thesis.

1.2.2 Confinement – the "Tokamak"

In the presence of a magnetic field, charged particles will experience a force perpendicular to their velocity and to the magnetic field. Because the force is always at a right angle to the velocity, it can not lead to an increase in the kinetic energy of the particle, but only change its direction. This means that the particles will be confined to move in orbits around the magnetic field lines, but they remain free to move parallel to the field. In order to fully confine the particles, the parallel motion has to be restricted as well. This can be accomplished by increasing the magnetic field at the edges of the device, creating what is called

[2] in physics, the term *fluid* is used for both liquids and gasses, as opposed to solids

[3] and, of course, Southern

[4] consider that Jupiter is in many ways a "failed" star: that the mass of the gas giant is too small to ignite its Hydrogen core illustrates the futility of gravitational confinement on Earth

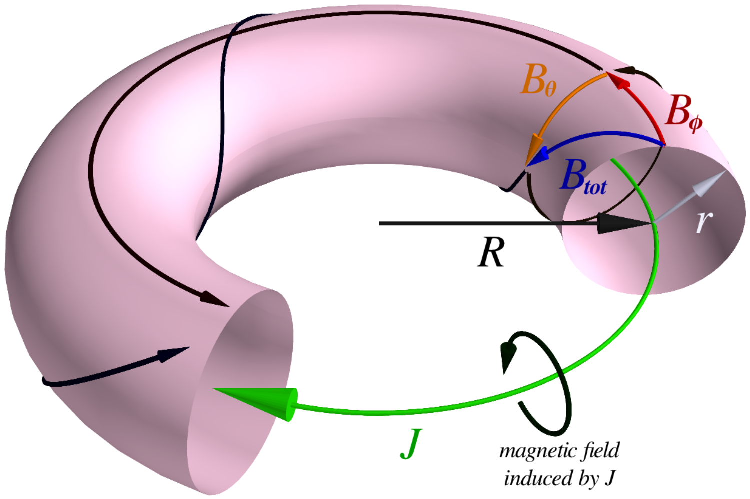

Figure 1.2: *Illustration of the origin of the helical magnetic field lines in a tokamak. The toroidal ($\boldsymbol{B}_\phi$; $\nwarrow$) and poloidal ($\boldsymbol{B}_\theta$; $\swarrow$) components of the total ($\boldsymbol{B}_{tot}$; $\leftarrow$) magnetic field are indicated. Neither $\boldsymbol{B}_\phi$ nor $\boldsymbol{B}_\theta$ have the necessary twist, but their sum $\boldsymbol{B}_{tot}$ is a field whose field lines spiral around the torus. This helicity has been exaggerated in the figure by choosing a safety factor $q \approx \frac{r}{R}\frac{B_\phi}{B_\theta} = 0.35$; for the scenarios in this thesis $q \sim 2$ typically. The surfaces spanned by the field lines of $\boldsymbol{B}_{tot}$ for different (minor) radii are referred to as* flux surfaces*. In most modern tokamaks these are not circular, see figure 1.3. The poloidal magnetic field is induced by the plasma current ($\boldsymbol{J}$; $\circlearrowright$) running along the toroidal axis of the plasma. Also indicated are the* major *($\boldsymbol{R}$; $\longrightarrow$) and* minor *(r; $\nearrow$) radii.*

a "magnetic mirror". Though this will cause many particles to bounce back into the core of the plasma, it can be shown that particle losses at the ends of the device are unavoidable [6]. Therefore, most research into potential power plant designs have been devoted to the study of toroidal magnetic geometries – instead of tying off the ends of the magnetic field, the field lines are bent into a ring, closing on themselves. The toroidal configuration is illustrated in figure 1.2.

Since the ends are eliminated this way, so are the end losses; however, this setup comes with its own difficulties, stemming from the inhomogeneity of the magnetic field. For a simple toroidal magnetic field, it can be shown that, due to a combination of effects due to the gradient and curvature of the magnetic field, the plasma will tend to be expelled from the core, toward the outside of the torus [6, 7]. This problem can be solved by introducing a twist (or "helicity") in the magnetic field, so that the field lines – and the particles following them – spend time on both the in- and the outside of the device. In that way, the particles pushed toward the edge of the plasma when on one side of the torus, will be pushed back into the core when on the other side.

The twist is created by adding a field in the poloidal direction to the toroidal field; their sum will be a field with field lines spiralling around the torus. Figure 1.2 presents an illustration of how the helical field lines are generated. The first method of inducing this twist utilised external coils for both the poloidal and the toroidal magnetic fields. The devices were called "stellarators", referring to the ambition of reproducing the workings of the sun and her stellar sisters here on Earth. Though stellarator research is a very active field (see e.g. [10, 11]), due to the difficulties of creating a favourable magnetic geometry by external means, most research since the sixties has shifted toward what is known as the "tokamak",[5] a configuration where the twist is accomplished by running a current through the core of the plasma. The current is induced by using the plasma – a very good conductor due to the free mobility of the electrons – as a the secondary winding of a transformer.[6] The relationship between the plasma current and the helicity of the magnetic field lines is illustrated in figure 1.2. This axial current then creates the poloidal field through Ampere's law [5]. The rate of the helicity is measured by a parameter called the *safety factor* (q), which can be seen as the number of toroidal turns a magnetic field line make in one poloidal turn. It is directly proportional to the ratio of the toroidal magnetic field strength (B_ϕ) to the poloidal magnetic field strength (B_θ) [13], see figure 1.2. For reasons of stability, the cross section of the plasma is not circular in modern tokamaks, but elongated and D-shaped, as illustrated in figure 1.3.

A drawback of this method of introducing a helical twist in the magnetic field is that the electromagnetic field driving the plasma current is proportional to the change in the magnetic flux, as described by Faraday's law of induction [5]. Therefore, the current can only be induced as long as the magnetic flux increases, which it cannot do indefinitely. Eventually the transformer core will saturate, and the plasma current can then no longer be sustained. Though there are advanced operating scenarios under investigation that may circumvent this, tokamak operations are currently limited to pulsed mode. This is not a problem

[5] "Tokamak" is an acronym for "*to*roidalnaya *ka*mera s *ma*gnitnaya *k*atushka", which is Russian for "toroidal chamber with magnetic coils" [2]. In some older works, however, one can instead read that it originates from "*to*roidalnaya *kam*era s *ak*sialnym magnitnym polem", or "toroidal chamber with axial magnetic field" [12]. Both acronyms are suitably descriptive of the device: the tokamak was developed in the Soviet Union in the middle of last century, and is indeed a toroidal chamber, with magnetic coils generating a magnetic field along the toroidal axis of the chamber. But this is common to all toroidal magnetic confinement devices – including stellarators – and so the name does not cut to the core of what sets the tokamak design apart from the others: the current creating the poloidal field.

[6] this also helps to heat the plasma through resistive (or "ohmic") heating, though at high temperatures the plasma is too good a conductor for this to be the only heating mechanism

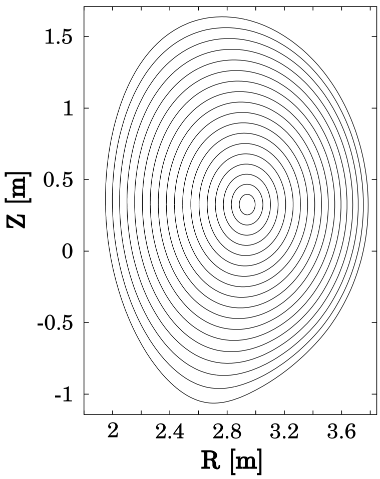

Figure 1.3: *The shape of the plasma cross section from JET experiment (discharge #67330). The image shows the surfaces of constant magnetic flux. The plasma shows a slight D-shape, with mostly elongation and low triangularity ($\kappa = 1.37$ and $\delta = 0.044$).*

for the study of plasma dynamics, which involve time scales much shorter than the pulse time, but certainly a drawback when it comes to power production.

1.2.3 Stability and quality of the confined plasma

Plasma confinement is a precarious process, only possible for precisely tuned parameters. One such parameter is the so called plasma β, which expresses the ratio of the particle pressure to the confining magnetic pressure. This parameter cannot exceed a few percent in tokamaks, or the plasma will be subject to large scale instabilities and disrupt, losing confinement almost at once [7, 13]. Pressure is related to the particle density and the temperature through the Boltzmann constant: $p = n_e k_B T$ [5].[7] Therefore, an increase in either the number of particles or temperature would proportionally increase the pressure, eventually bringing it above the β-limit.

Though the β-limit puts a severe constraint on the operating regimes available to achieve fusion power, it also makes the process inherently safe from anything like a nuclear melt-down. "Disruption" and "loss of confinement" may sound dire enough, considering that the temperature of the plasma can reach in excess of a hundred million degrees Celsius. The actual energy content of the plasma, however, is very modest, which can also be seen from the definition of pressure. Dimensionally, pressure is a measure of the energy density in a fluid. For a

[7]the subset $_e$ is for *electrons*, which is conventionally used, since the electron density in a fully ionised gas is a measure of the ion density, regardless of the number of ion species

typical fusion plasma in ITER [14], the particle density will be $n_e \approx 10^{20}\,\mathrm{m}^{-3}$ for a volume of $V \approx 10^3\,\mathrm{m}^3$, and the temperature will be roughly $T \approx 10^8\,\mathrm{K}$. With $k_B \approx 10^{-23}$ J/K, combining these gives an energy density of approximately 10^5 J/m^3. This is equivalent to 10^3 kPa, which is of the same order as the normal atmospheric pressure at sea level.[8]

Based on the energy content of the plasma, a measure of the quality of the confinement can be defined as the quotient of the energy content E and the power input P_{in} needed to sustain the plasma at that level of energy: $\tau_E \equiv E/P_{in}$, which has the dimension time. This is a measure of how quickly the energy would be lost, if power were not supplied, and is therefore called the *energy confinement time*. By dimensional arguments it can be shown that the power balance leads to a requirement for net energy production of $\tau_E n_e > (\tau_E n_e)_c$, for some critical value $(\tau_E n_e)_c$ [13]. This is called the *Lawson criterion*, and expresses the condition for power *break-even*. A more concrete performance parameter is that of the "fusion triple product": $n_e T \tau_E > (n_e T \tau_E)_c$, valid in the temperature range considered for fusion. The triple product is a condition for a self sustained plasma, meaning that the necessary power to heat the plasma comes from the α particles generated by fusion events.[9] In fusion experiments, the achieved triple product has been increasing exponentially over time since the dawn of fusion research, and the ITER device currently under construction is expected to continue this trend, with an estimated output power of five to ten times the input power [3, 7, 14]. Because of stability requirements, such as the β-limit mentioned above, the particle density and temperature are both restricted. Therefore, significantly increasing the Lawson parameter or the fusion triple product requires increasing the energy confinement time, which requires an understanding of the transport mechanisms at work.

1.3 Plasma impurities

Impurities – any ions that are not part of the fuel – tend to dilute the fuel, making collisions that produce fusion rarer, and thus reducing the fusion power. Heavier elements also tend to cool the plasma through radiative processes. Their high nuclear charge make them hard to ionise fully, even at the temperatures of a fusion plasma, and the electrons remaining bound to the impurity can then, rather than separate from the nucleus, respond to a collision by jumping to a higher electron orbit [15]. As the electrons relax, returning to the lower energy levels, they lose the energy gained in the collision, which is released in the form of photons. This is called *line radiation*, because the frequencies of the released

[8] the energy associated with the free electrons has been neglected here: the ionisation energy for Hydrogen is ~ 10 eV, which translates to roughly 10^2 J/m^3, so this contribution is negligible compared to the thermal energy of the ions

[9] both the Lawson criterion and the fusion triple product are valid measures of the quality of fusion plasmas for magnetically as well as inertially confined fusion plasmas, but in magnetic confinement fusion n_e is typically small and τ_e large, while the opposite holds for inertial confinement fusion

photons correspond to lines in the light spectrum characteristic to the element that produced them. Since some heavy elements may never be fully ionised, line radiation can continue indefinitely. Therefore, even a small dilution of heavy impurities, can lead to significant energy losses in the plasma.

There are mainly three potential sources of impurities: the first being the walls of the reactor chamber. Due to the different roles played by different parts of the walls, they contribute both light and heavy impurities. The divertors, for instance, need to withstand the heavy power loads from energetic particles, and are therefore made of heavy metals such as Tungsten (W; nuclear charge $Z = 72$). Because of the danger of line radiation, using an element as heavy as Tungsten is not practical for all of the chamber, and hence lighter candidates with high heat resilience are used elsewhere. For example, at the Joint European Torus (JET, [16]) the new ITER-like wall project was recently initiated, testing the feasibility of using a coating of the light metal Beryllium (Be, nuclear charge $Z = 4$) on the plasma facing first wall of the reactor chamber [17].

Not all impurities, however, are contaminants. The second main source of plasma impurities is injections of particles for control purposes. Here the cooling mechanisms are beneficial to the operation of the fusion reactor. By injecting inert gasses such as Argon (Ar, $Z = 18$) that radiate energy, the heat load on components such as the divertors can be spread out, protecting them from wearing out [18]. Impurities are also injected for experimental purposes, in order to study their transport properties.

Finally, the fuel ions will, in a working power plant, be diluted by the steady production of α-particles (sometimes referred to as "Helium ash") through fusion reactions.

Of major concern is the transport properties of heat, momentum and particles, e.g. whether different kinds (or "species") of impurities will experience an inward or an outward transport. Simulations of this is the main topic in this thesis.

1.4 Transport processes

Understanding the transport of particles, heat, momentum etc. in fusion plasmas is a very important topic of research. As mentioned above, controlling the transport properties of the plasma may be the only way forward when it comes to increasing the fusion efficiency, as measured by the Lawson parameter and the fusion triple product (section 1.2.3).

In fluids, it is common to describe the transport as consisting of diffusion and convection.[10] Diffusion is the (seemingly) random spreading of a quantity in a fluid. It can often be understood as being mediated by collisions in the flow leading to a dispersive random walk [19]. Diffusive transport is driven by gradi-

[10] advection is often used in place of convection, using convection to mean the sum of advective and diffusive transport

ents, and so diffusion is directed from areas of abundance, to areas of scarcity. Thereby diffusion tends to even out profiles of temperature, density etc.

The convective part of the transport relates to bulk motion of particles in a fluid. It can either be up or down gradient, depending on the situation. In fusion plasmas, an net convective velocity is often referred to as a “pinch”.

Transport is often separated into *classical* and *anomalous* transport, where classical refers to transport dominated by collisions, whereas all other observed transport is termed anomalous [20]. Experiments have shown that, for most regions of the fusion plasma, anomalous transport clearly dominates over classical transport [20]. The most common example of anomalous transport in plasmas is turbulent transport. Turbulence is often associated with strong gradients, which represent free energy within a system that can drive instabilities. It is difficult to envision any situation in Classical Physics, where the gradients are more pronounced than in a modern magnetic confinement fusion device; however, turbulence is a very common phenomenon in all of Nature. This has therefore been a topic of study for scientists and engineers for the better part of three hundred years, but its nonlinear character means that studying the effects of turbulence is very challenging. One main feature of turbulence is the interaction and interchange between different time and length scales, meaning that turbulent transport cannot be properly described by simple convection and diffusion. Locally, however, this approximation can be valid, when looking at space and time averaged fluxes [21–24]. The turbulent transport then manifests itself as effective diffusivities and pinches, valid for particular minor radii.

All turbulent dynamics exhibit nonlinearities, making exact analytical solutions to equations of motion hard to come by. This necessitates the application of numerical methods. To aid researchers when predicting and interpreting experimental outcomes, numerical tools have been developed to study the transport. Both dedicated transport solvers and more general plasma codes are used to this end. The study of plasma physics using such tools is the main topic in this thesis.

2

Turbulent particle transport

2.1 ITG and TE mode turbulence

In most regions of fusion plasmas, turbulent transport dominates over classical transport [20]. This turbulence has important and non-trivial effects on e.g. the quality of the energy confinement – effects that are hard to tackle both analytically and numerically.

The origin of turbulent transport in tokamak plasmas is fluctuations in the plasma. Crucially, the magnitude of the transport does not only depend on the the magnitude of the fluctuations, but also on the extent of the phase correlation between the fluctuating quantities. For instance, for a net particle flux, the fluctuation in the velocity field needs to be accompanied by a fluctuation in the particle density that is correlated with the velocity fluctuation.

For the linear modes driving the turbulence considered in this thesis – ion temperature gradient (ITG) and trapped electron (TE) modes in low β plasmas – the perturbation can can be considered to be mainly electrostatic. Both the ITG and the TE mode are examples of so called reactive drift wave modes, a class of low frequency micro-instabilities, driven by the free energy associated with the gradients of temperature and density. They are both associated with length scales known to cause transport ($k_\theta \rho_s \approx 0.3$),[1] and their mode frequencies are of the same order as the magnetic and diamagnetic drift frequencies ($\omega_r \sim \omega_D$, ω_*).

These instabilities can be understood as analogous to the Rayleigh–Taylor instability, where a dense fluid is supported by a less dense fluid against the influence of gravity [6, 7, 13]. This is the case on the low-field outboard side of the toka-

[1] Please see table 2.1 for some definitions used throughout this chapter!

Table 2.1: *A collection of plasma quantities used in the text; † denotes particle drifts*

ρ_j	$\sqrt{\frac{T_j}{2m_j\Omega_{cj}^2}}$	Larmor radius of species j
ρ_s	$\sqrt{\frac{T_e}{m_i\Omega_{ci}^2}}$	Larmor radius at sound speed
v_{Tj}	$\sqrt{\frac{T_j}{2m_j}}$	thermal velocity for species j
c_s	$\sqrt{\frac{T_e}{m_i}}$	ion sound speed
Ω_{cj}	$\frac{q_jB}{m_j}$	cyclotron frequency for species j
$\omega_{Dj} = \boldsymbol{k}\cdot\boldsymbol{v}_{Dj}$	$2\frac{k_\perp T_j}{q_jB}\frac{\nabla B}{B}$	magnetic (∇B+c) drift frequency for species j
$\omega_{*j} = \boldsymbol{k}\cdot\boldsymbol{v}_{*j}$	$\frac{k_\perp T_j}{q_jB}\frac{\nabla n_j}{n_j}$	diamagnetic drift frequency for species j
$\boldsymbol{v}_E$	$\frac{\boldsymbol{E}\times\boldsymbol{B}}{B^2}$	$\boldsymbol{E}\times\boldsymbol{B}$ drift velocity†
$\boldsymbol{v}_{\nabla Bj}$	$\frac{\mu}{m_j\Omega_{cj}}\frac{\boldsymbol{B}\times\nabla B}{B}$	∇B drift velocity for species j†
$\boldsymbol{v}_{cj}$	$\frac{v_\parallel^2}{\Omega_{cj}B}\frac{\boldsymbol{B}\times\nabla B}{B}$	curvature drift velocity for species j†

mak, which for its propensity for driving instabilities is called the *bad curvature region*. The poloidal variation of the density and temperature perturbations will therefore have maxima on the outside, and minima on the inside, which is referred to as *ballooning* [7, 25]. The perturbations associated with these instabilities are such that $\delta X_j/X_j \ll 1$, but $\nabla\delta X_j/\nabla X_j \sim 1$, where X is e.g. temperature (T_j) , density (n_j) or electric potential (ϕ).

The ITG mode is destabilised when the ratio between the density and temperature gradient scale lengths, $\eta_i = L_{n_i}/L_{T_i}$ exceeds a critical value, which is typically of the order $\eta_i \approx$ 3–5. This instability is therefore commonly referred to as the *η_i-mode*. The instability can be understood as arising from a fluctuation in the temperature (δT_i), which under the influence of the poloidal magnetic drift causes a response in the ion density. Ions in regions perturbed to a higher temperature will have a higher magnetic drift velocity. A density perturbation (δn_i) is thus formed, where ions congregate downwind of the positive temperature perturbations, while the upwind side is depleted.

Assuming that δT_i is periodic, δn_i is therefore out of phase with δT. The electrons, on the other hand, can be considered adiabatic, and their density perturbation follows the Boltzmann distribution, with $\delta n_e/n = e\delta\phi/T_e$. This perturbation is in phase with δn_i in order to fulfil quasineutrality (equation (2.8)). The electrostatic potential $(\delta\phi)$ associated with δn_e results in an electric field $(\boldsymbol{E})$ across δT_i in the poloidal direction. This will in turn lead to a drift velocity perpendicular to $\boldsymbol{E}$ and to the magnetic field $(\boldsymbol{B})$, i.e. in the radial direction. This drift is the $\boldsymbol{E}\times\boldsymbol{B}$ drift $(\boldsymbol{v}_E)$. It will act on the temperature perturbation, and thus closing the feedback loop.

In the bad curvature region the effect is such, that hot particles will be transported out into the already hot areas, while cold particles from further out are transported in to the colder regions, thus creating a positive feedback.

The origin of the TE mode instability is qualitatively similar in nature to the origin of the ITG mode, but here the electrons trapped in banana orbits in the bad curvature region participate, taking the role of the ions. Whereas the ITG mode is destabilised by the ion temperature gradient, the TE mode instability can be driven by both the electron density and temperature gradients.

2.2 Kinetic description of the fusion plasma

Deriving expressions for the drift velocities and the density responses etc. can be done using different theoretical frameworks. In kinetic theory the plasma is described through distribution functions of velocity and position for each of the included plasma species. The principal equation for describing the time-evolution of the particle distribution functions is the Fokker–Planck (or Boltzmann) equation. For species j – main ions, electrons and impurities – this is written

$$\frac{\partial f_j}{\partial t} + \boldsymbol{v} \cdot \nabla_{\boldsymbol{x}} f_j + \frac{e_j}{m_j} \left(\boldsymbol{E} + \boldsymbol{v} \times \boldsymbol{B} \right) \cdot \nabla_{\boldsymbol{v}} f_j = C_j \left(f_j \right), \tag{2.1}$$

where $f_j = f_j(\boldsymbol{x}, \boldsymbol{v})$ is the distribution function, e_j and m_j are the charge and mass of the species, and $\boldsymbol{E}$ and $\boldsymbol{B}$ are the total electric and magnetic fields, including small scale perturbations. $C_j(f_j)$ on the right hand side contains a collision operator which describes the Coulomb interactions of the particles. When this is neglected, the equation is often referred to as the Vlasov (or collisionless Boltzmann) equation.

The electric and magnetic fields are determined by Maxwell's equations [5]:

$$\nabla \cdot \boldsymbol{E} = \sum_j \frac{\rho_j}{\epsilon_0}, \tag{2.2}$$

$$-\mu_0 \epsilon_0 \frac{\partial \boldsymbol{E}}{\partial t} + \nabla \times \boldsymbol{B} = \sum_j \mu_0 \boldsymbol{j}_j, \tag{2.3}$$

$$\nabla \cdot \boldsymbol{B} = 0, \tag{2.4}$$

$$\nabla \times \boldsymbol{E} + \frac{\partial \boldsymbol{B}}{\partial t} = 0. \tag{2.5}$$

These couple to equation (2.1) through the charge density (ρ_j) and current ($\boldsymbol{j}_j$), which are obtained from the zeroth and first order velocity moments of the particle distribution function (f_j):

$$\rho_j \left(\boldsymbol{x} \right) = q_j n_j \left(\boldsymbol{x} \right) = q_j \int \mathrm{d}^3 \boldsymbol{v} \, f_j \left(\boldsymbol{x}, \boldsymbol{v} \right), \tag{2.6}$$

$$\boldsymbol{j}_j \left(\boldsymbol{x} \right) = q_j n_j \left(\boldsymbol{x} \right) \boldsymbol{v}_j \left(\boldsymbol{x} \right) = q_j \int \mathrm{d}^3 \boldsymbol{v} \, \boldsymbol{v} f_j \left(\boldsymbol{x}, \boldsymbol{v} \right), \tag{2.7}$$

where q_j is the charge of species j.

For the ion-scale low-frequency phenomena of interest in this thesis, Gauss' equation (equation 2.2) is replaced to lowest order by quasineutrality [7]:

$$\sum_j q_j \delta n_j \approx 0. \tag{2.8}$$

In electrostatic cases ($\beta \approx 0$), the situation is further simplified, in that only quasineutrality is necessary to get the density responses.

2.2.1 Gyrokinetics

Equation (2.1) together with the Maxwell equations give a complete description of the time evolution of the plasma, however, for the purpose of turbulence modelling some simplifications are useful. The kinetic equations are inherently six-dimensional; however, in magnetically confined fusion plasmas the confined particles are generally constrained to fast orbits along field lines. This motivates performing an average over the gyration, reducing the problem to five-dimensional gyrokinetic equations [26–29]. Since the equations governing the evolution of the distributions are all coupled, the resulting decrease in numerical complexity is considerable. Even more importantly, the gyro-average relaxes the need to temporal scales much shorter than the inverse ion cyclotron frequency ($1/\Omega_{ci}$).

There are some requirements that need to be fulfilled, for this simplification of the equations to be appropriate. First of all, the Larmor gyro-radii (ρ) of the plasma species have to be small compared to the system size and gradient scale lengths (R, L_n and L_T), and the associated cyclotron frequencies (Ω) have to be large compared to the frequency of the turbulent fluctuations (ω). Second, the fast motion of the particles along the field lines lead to the requirement that the typical wave length of the parallel structure of the turbulence ($1/k_\parallel$) is much longer than the perpendicular ditto ($1/k_\perp$) Finally, the energy associated with turbulent fluctuations ($q\delta\phi$) needs to be small compared to the thermal background energy (T). The first condition defines a *smallness parameter* $\epsilon \equiv \rho/R$, and all the ratios are taken to be of this order. This is called the gyrokinetic ordering, which generally holds for the core of tokamak plasmas, but may be inappropriate nearer the edge [27, 30]. Formally, this can be written:

$$\epsilon = \frac{\rho}{R} \sim \frac{\rho}{L_n} \sim \frac{\rho}{L_T} \sim \frac{\omega}{\Omega} \sim \frac{k_\parallel}{k_\perp} \sim \frac{q\,\delta\phi}{T} \ll 1. \tag{2.9}$$

By performing the average of the particles' gyrations around the field lines, keeping terms up to $\mathcal{O}(\epsilon)$, an equation following the centre of the gyration – the guiding centre $\boldsymbol{X}$ – rather than the explicit orbits can be obtained. This reduces the velocity space coordinates from three to two directions: parallel velocity ($v_\parallel$) and magnetic moment ($\mu = m_j v_\perp^2/2B$). Neglecting collisions, μ becomes an adiabatic invariant and can be treated as a parameter, further reducing the problem by one dimension. In this limit, the gyrokinetic Fokker-Planck equation can be written [31]:

$$\frac{\partial F_j}{\partial t} + \left(\boldsymbol{v}_\parallel + \frac{B_0}{B_{0\parallel}^*} \left(\boldsymbol{v}_E + \boldsymbol{v}_{\nabla B_0} + \boldsymbol{v}_c \right) \right) \cdot \left(\nabla F_j + \frac{1}{m_j v_\parallel} \left(q_j \delta \boldsymbol{E} - \mu \nabla \left(B_0 + \delta \bar{B}_\parallel \right) \right) \frac{\partial F_j}{\partial v_\parallel} \right) = \bar{C}_j(F), \quad (2.10)$$

where $F_j(\boldsymbol{X}, v_\parallel, \mu)$ is the gyro-averaged distribution function, $\delta\boldsymbol{E}$ and $\delta\boldsymbol{B}$ are the perturbed electric and magnetic fields, $B_{0\parallel}^* = (\nabla \times (\boldsymbol{A}_0 + \frac{m_j}{q_j B_0} v_\parallel \boldsymbol{B}_0)) \cdot \boldsymbol{B}_0 / B_0$, and over-bar denotes gyroaveraging; the particle drift velocities can be seen in table 2.1, where $\boldsymbol{E}$ in $\boldsymbol{v}_E$ should be replaced by $-\nabla\chi_j$, the gradient of the gyro-modified potential $\chi_j = \bar{\phi} + v_\parallel \delta \bar{A}_\parallel + (1/q_j)\delta \bar{B}_\parallel$.

This equation together with the gyroaveraged Maxwell's equations for the perturbed fields ((2.3)–(2.5)) form the gyrokinetic description of turbulent transport. As state above, quasineutrality (equation (2.8)) can safely replace Gauss' law (equation (2.2)) for the spatial scales considered in this thesis.

2.3 Fluid description of the plasma

By calculating the velocity moments of the particle distribution function, fluid quantities such as density, pressure etc. can be obtained. The zeroth and first moments are the density (n_j) and velocity ($\boldsymbol{v}_j$). These were calculated in equations (2.6) and (2.7) above. The dynamics are obtained in the same way, by taking the moments of the Fokker–Planck equation. The zeroth, first and second order moment yields the equations of *continuity*, *momentum balance* and *energy* [7, 32]:

$$\frac{\partial n_j}{\partial t} + \nabla \cdot (n_j \boldsymbol{v}_j) = 0. \quad (2.11)$$

$$m_j n_j \frac{\partial \boldsymbol{v}_j}{\partial t} + m_j n_j \boldsymbol{v}_j \cdot \nabla \boldsymbol{v}_j = n_j q_j \left(\boldsymbol{E} + \boldsymbol{v}_j \times \boldsymbol{B} \right) + \nabla p_j - \nabla \cdot \boldsymbol{\Pi}_j, \quad (2.12)$$

$$\frac{3}{2} \left(\frac{\partial}{\partial t} + \boldsymbol{v}_j \cdot \nabla \right) p_j + \frac{5}{2} p_j \nabla \cdot \boldsymbol{v}_j + \boldsymbol{\Pi}_j : \nabla \boldsymbol{v}_j + \nabla \cdot \boldsymbol{q}_j = 0, \quad (2.13)$$

where $\boldsymbol{\Pi}_j$ is the stress tensor and : is the inner tensor product, $\boldsymbol{q}_j$ is the heat flux, p_j is the plasma pressure, and collisions and sources have been neglected. As can be seen in equation (2.11), the zeroth order equation depends on the first order moment. It is a property of all the moment equations, that they depend on a higher order moment, wherefore the system needs to be truncated by an appropriate closure in order to be tractable [7]. In the Weiland model, used in Paper **I**, Paper **II** and Paper **III**, the fluid hierarchy is truncated at the diamagnetic heatflow, with [7]:

$$\boldsymbol{q}_j = \boldsymbol{q}_{*j} = \frac{5}{2}\frac{p_j}{m_j \Omega_{cj}}\frac{\boldsymbol{B}\times\nabla T_j}{B}. \tag{2.14}$$

In addition to making the workings of the plasma more accessible, by reintroducing familiar physical concepts such as pressure and density, fluid models are also several orders of magnitude more computationally efficient. There are however inherently kinetic effects that are not reproduced by fluid models, most notably kinetic resonances that are important in many circumstances.

2.4 Transport

In the case of a purely electrostatic perturbation, the particle flux of ion species j can formally be written [20]:

$$\Gamma_j = \langle \delta n_j v_E \rangle \,, \tag{2.15}$$

where δn_j is the perturbation in the density of species j and v_E is the $\boldsymbol{E}\times\boldsymbol{B}$ drift velocity [7]. The angled brackets imply a time and space average, which includes contributions from ITG and TE modes. Performing the average in equation (2.15) for a fixed length scale $k_\theta \rho_s$ of the turbulence, leads to an expression of the following form:

$$\frac{R\Gamma_j}{n_j} = D_j\frac{R}{L_{n_j}} + D_{T_j}\frac{R}{L_{T_j}} + D_u\frac{R}{L_u} + RV_{p,j}. \tag{2.16}$$

The first term on the right hand side of equation (2.16) corresponds to ordinary diffusion, while the next three together form the off-diagonal pinch. The second term is thermodiffusion, the third roto-diffusion, and the third is the convective velocity or "pure convection". Here $R/L_{X_j} = -R\nabla X/X$, where $X = n_j$, T_j, u, are the logarithmic gradients of density and temperature for species j, and of the toroidal velocity profile, normalised to R – the major radius of the tokamak. The pinch here contains contributions from curvature and parallel compression effects, however, the thermodiffusive term in equation (2.16) is sometimes referred to as the thermopinch and included in the convective velocity, so as not to confuse it with the proper (i.e. density gradient driven) diffusion. These terms have been described in detail in previous works, see e.g. [21–23] and Paper **I** and Paper **II** in this thesis.

In general equation 2.16 is not linear, since the diffusion coefficients and the convective pinch term depend on the gradients. There is, however, an important special case – *trace impurities* – where the relation is truly linear. For trace amounts of an impurity Z,[2] the impurity dynamics have no effect on the turbulence, and therefore D_Z, D_{T_Z}, D_u and $V_{p,Z}$ are independent of the impurity

[2] Z refers to the charge number of the impurity

gradients [21]. The relationship of PF to D_Z and $RV_Z = D_{T_Z} R/L_{T_Z} + RV_{p,Z}$ is illustrated in figure 3.3.

2.5 Peaking factors

In the core of a steady-state plasma with fuelling from the edge (i.e. no internal particle sinks or sources), the particle flux Γ_j will go to zero. Solving equation (2.16) for R/L_{n_j} with $\Gamma_j = 0$ yields the steady-state gradient of zero particle flux. Since this is a measure of how peaked the density profile is at steady state, we refer to this as the *peaking factor* for species j:

$$PF_j \equiv \left.\frac{R}{L_{n_j}}\right|_{\Gamma=0} = -\frac{RV_j}{D_j}, \tag{2.17}$$

where V_j is the total pinch, including contributions from the thermopinch and roto-diffusion. As can be seen on the right hand side of the equation, this is a measure of the balance between convective and diffusive particle transport.[3] Specifically, the sign of the peaking factor is determined by the sign of the pinch, meaning that $PF_j > 0$ is indicative of a net inward particle pinch, giving a peaked density profile. Conversely, if $PF_j < 0$ the net particle pinch is outward, leading to a hollow density profile. The latter condition is called a *flux reversal*, and conditions leading to this are of particular interest for impurity transport, since an accumulation of impurities in the core of the plasma should preferably be avoided (see section 1.3).

Since, as discussed in section 2.1 above, equation 2.16 is linearly dependent on the impurity density gradient in the trace impurity limit, equation 2.17 can be solved by computing the impurity flux for different values of R/L_{n_Z}. This is detailed in section 3.2.2 and illustrated in figure 3.3. The contribution to PF_Z from the thermopinch can be found by similar means, as discussed in section 3.2.3 and illustrated in figure 4.3.

2.6 Contributions to the convective pinch

Much of the observed variation in the impurity transport – in particular the difference between TE and ITG mode dominated cases – can be understood from the convective velocity $V_j = D_{T_j} 1/L_{T_j} + V_{p,j}$ in equation (2.16). It has been observed that both the pure convection and the thermodiffusion have opposite signs for electrons and impurities in both ITG mode and TE mode driven turbulence [35, 36]. Specifically, in the curvature/∇B driven branches of the instabilities, which are the branches studied in this thesis, we have [36]:

- thermodiffusion (D_{T_j}) is

[3]this number is also sometimes referred to the *Péclet number* [33, 34]

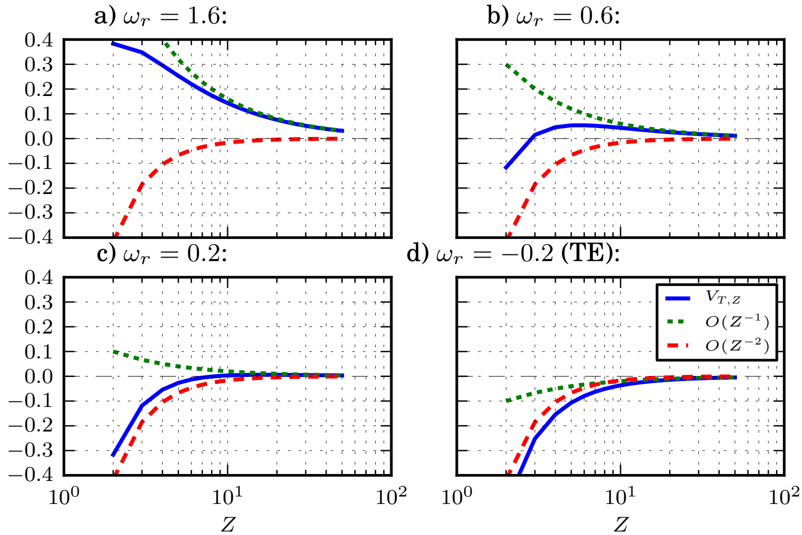

Figure 2.1: *Illustration of the importance of the second order contribution to the impurity thermopinch ($D_{T_Z} 1/L_{T_Z}$; equation (2.18)) for different real frequencies (ω_r). In the ITG mode driven case, the impurity thermopinch is strictly outward ($D_{T_Z} 1/L_{T_Z} > 0$) for high mode frequencies (*a*), but changes to inward ($D_{T_Z} 1/L_{T_Z} < 0$) for lower charge numbers (Z) as ω_r is reduced and the second order term comes into dominance (*b*), until it is mostly negative (*c*). For the TE mode driven case (*d*) $\omega_r < 0$, wherefore the thermopinch is inward for all impurities.*

  – inward for electrons and outward for impurities in ITG mode,
  – outward for electrons and inward for impurities in TE mode,

- pure convection ($V_{p,j}$) is inward for electrons and impurities in both modes,
- collisions create an outward electron and impurity pinch in ITG mode and an inward electron and impurity pinch in TE mode,
- sheared toroidal rotation creates an outward electron and impurity pinch in ITG mode and an inward impurity pinch in TE mode.

For the impurity transport, it is possible to make a more quantitative analysis. The pinch contains two terms that to lowest order depend on the impurity charge number Z. These are [21] the thermopinch ($D_{T_Z} \sim 1/Z$) and parallel impurity compression ($V_{\parallel,Z} \sim (Z/A_Z)\, k_\parallel^2 \sim Z/\left(A_Z q^2\right) \approx 1/\left(2q^2\right)$). Here $1/k_\parallel$ decides the wavelength of the parallel structure of the turbulence. Due to the ballooning character of the modes considered, this is proportional to the safety factor (q). The direction of these contributions to the pinch are governed mainly by the considered mode's drift direction, which is different for TE and ITG modes [7].

The Z dependence in the parallel impurity compression is expected to be weak, since the mass number is approximately $A_Z \approx 2Z$ for an impurity species with charge Z. The thermodiffusive contribution, however, can dominate the transport for low Z impurities (such as the Helium ash and Beryllium from the wall), thereby qualitatively explaining the observed Z scalings of the impurity peaking factor seen in the appended articles. To see this, we look at the second order correction to the thermopinch, which can become important for low charge numbers. Neglecting finite Larmor-radius effects and expanding the kinetic integral to first order in ω/ω_D, the thermopinch to second order goes as [7, 21, 24, 37]:

$$D_{T_Z} \frac{R}{L_{T_Z}} \sim \left(\omega_r \frac{T_Z}{T_e Z} - \frac{7}{4} \left(\frac{T_Z}{T_e Z} \right)^2 \right) \frac{R}{L_{T_Z}}. \tag{2.18}$$

Whereas the first order term is proportional to the driving mode's real frequency (ω_r), and therefore outward for ITG modes ($\omega_r > 0$) and inward for TE modes ($\omega_r < 0$), the second order term is inward, independent of the mode direction. This means that for light impurities and low enough mode frequencies, the ITG mode driven thermopinch can change direction from outward to inward, thereby increasing PF_Z. This is illustrated in figure 2.1 and discussed in detail in Paper **II** and Paper **IV**.

3

Gyrokinetic simulations

3.1 Experiments in silico

The GENE code [30, 31, 38, 39] is a massively parallel gyrokinetic Vlasov code, solving the nonlinear time evolution of the gyrokinetic distribution functions on a fixed grid in phase space. In real space, the radial (x) and bi-normal (y) dependencies are treated spectrally, i.e. those directions are discretised explicitly in k-space, whereas the toroidal (z) direction is discretised in real space.

In this work, GENE simulations were performed in a flux tube geometry with periodic boundary conditions in the perpendicular directions. The flux tube is in essence a box that is elongated and twisted along with the $\boldsymbol{B}$ field as the field lines traverse the tokamak, thus covering the poloidal and parallel dimensions. Its application relies on the assumption that the scales of the phenomena of interest are all small compared to the size of the flux tube. The periodic boundary conditions also imply the assumption, that local effects dominate over global. This may be true for some kinds of turbulence, whereas other modes have definite global characteristics. An alternative simulation domain is the 'toroidal annulus' which explicitly resolves the poloidal direction as well, but retains the assumption of locality in the radial direction. However, the advantage of this over the flux tube domain is limited, and what is really required in order to investigate the validity of the locality assumption is a global simulation domain, where gradients etc. are allowed to vary with radius. With the steady advance of computer resources, global simulations of plasmas are becoming feasible; however, this is outside the scope of this thesis.

The instantaneous memory usage of a nonlinear GENE simulation is often of the order of several gigabyte. This means that even conservatively saving run-time data is unfeasible. Instead, GENE reduces the raw field data to physically comprehensible fields, which are saved to disk at intervals specified by the user. An example of this is shown in figure 3.1, where a cross section of the simulation domain is shown. The highlighted area corresponds to a cross section of the flux tube, whereas the rest of the annulus is approximated from the whole three-dimensional data set. The quantity shown is the fluctuations in the electrostatic potential ϕ near the end of a TE mode simulation. The saved data can be loaded into e.g. GENE's native diagnostics tool, and after further refinement, data for specific physical quantities can be extracted.

Images such as the one presented in figure 3.1 are useful for providing quick "sanity checks" for the simulations:

- Are the turbulent features sufficiently small, compared to the domain size?
- Are they large enough, compared to the resolution?
- Are there features that look artificial?

Beyond that, however, the derived data is still difficult to compare directly with experiments – numerical and physical alike – before it has been further distilled. By performing different averages over the simulation domain, scalar quantities are derived, such as mean fluctuation levels of particle densities and of the electrostatic potential, and integrated particle and heat fluxes across the flux tube. Since such scalar quantities are often what is needed for further analysis, GENE by default calculates and saves a number of such averages at regular intervals. Because they are scalars rather than fields, the resulting time-series can afford a very good temporal resolution, without hampering simulation performance or running out of disk space. Two such time-series are presented in figure 3.2. They show the space averaged fluctuations in background ion density (n_{H}^2) and impurity flux ($\mathit{\Gamma}_Z$) for the same simulation as in figure 3.1.

GENE can also be run in quasilinear mode, a method that is considerably less demanding when it comes to computer resources since the non-linear coupling between length scales is ignored [31, 39, 40]. Here, the method is only used to study one mode at a time, and only for the particular length scale $k_\theta \rho_s$ of choice. If the length scale is chosen appropriately, however, the quasilinear simulation will capture the essential features of the dynamics, and it is useful for getting a qualitative understanding of the physical processes. As used in this work, it captures the contribution from the most unstable mode, not from any sub-dominant modes. In the following, the methodology is the same as for both kinds of simulations.

3.2 Post-processing

3.2.1 Time averaged quantities

In order to study the quantities of principal interest in this thesis the data needs to be condensed into comprehensible quantities. The methods used to obtain these are described in some detail in this section.

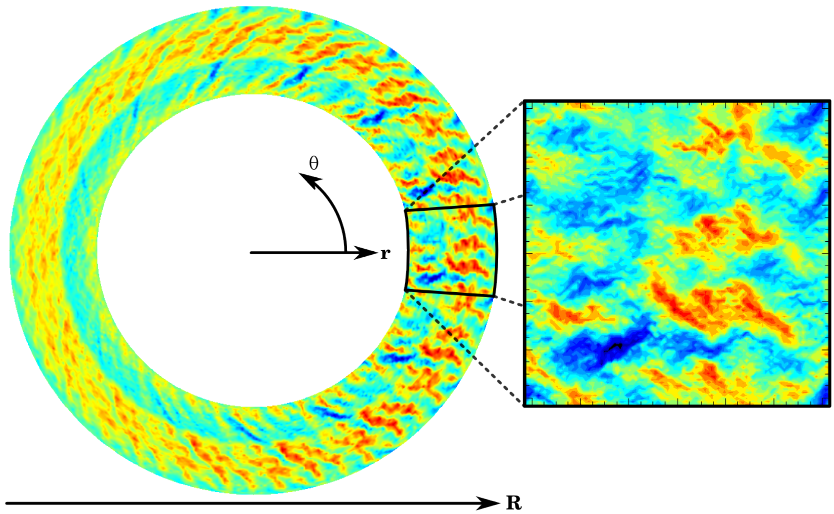

Figure 3.1: *A cut from the toroidal annulus made up of the flux tube as it twists around the torus following the $\boldsymbol{B}$ field; see figure 1.2. Shown are the fluctuations in the electrostatic potential (ϕ). A cross-section of the flux tube with the side $\sim 125\,\rho$ is indicated. Data from NL GENE simulation of TE mode turbulence at $t \approx 300\,R/c_s$; parameters as in figure 4.1a.*

For non-linear simulations, the starting point for the analysis is usually an averaged quantity, such as mean impurity flux: $\langle \Gamma_Z \rangle$. Because the time-step in the simulation is variable, a simple average of the data does not suffice. Instead, a weighted average is performed, using the time-steps as weights:

$$\langle \Gamma_Z \rangle = \frac{\displaystyle\sum_{n=n_0}^{N} \frac{t_{n+1} - t_{n-1}}{2} \Gamma_{Z,n}}{\displaystyle\sum_{n=n_0}^{N} \frac{t_{n+1} - t_{n-1}}{2}} = \frac{\displaystyle\sum_{n=n_0}^{N} \left(t_{n+1} - t_{n-1}\right) \Gamma_{Z,n}}{t_{N+1} - t_{n_0-1}}. \tag{3.1}$$

Here $\Gamma_{Z,n}$ is the flux sampled at time t_n, and times $t < t_{n_0}$ are discarded to ensure that the turbulence has reached saturation.[1] This is illustrated in 3.2, where an uncertainty for the mean flux of $\pm$ one standard error has been indicated. Though the average is fairly straight forward to compute, this uncertainty is more subtle.

For N independent samples x_i from a Gaussian process, the standard error σ of the mean μ can be sought as $\sigma \approx \sqrt{\mathrm{Var}[x_i]/N}$. There are two reasons why this cannot be used directly in gauging the uncertainty of our time-series:

1. the process is not a symmetric Gaussian, as can be seen from the bursty nature of the time-series in 3.2;

[1] note that the $(N+1)$th sample is also discarded, and only the time stamp is used

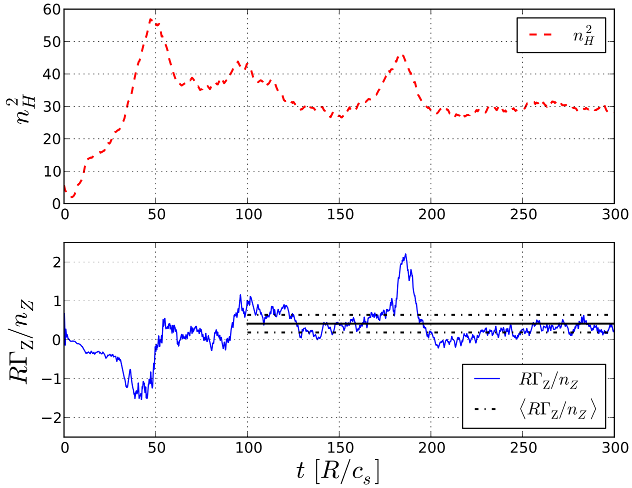

Figure 3.2: *Time series showing fluctuations in the main ion density (n_H^2) and impurity flux (Γ_Z) after averaging over the whole flux tube; see figure 3.1. The average impurity flux ($\langle\Gamma_Z\rangle$) is calculated from Γ_Z, discarding the first portion so as not to include the linear phase of the simulation. $\langle\Gamma_Z\rangle$ is used for finding the peaking factor for the impurity species; see figure 3.3. NL GENE simulation with He impurities; parameters as in figure 4.1a, with $R/L_{n_Z} = 1.5$. An estimated uncertainty of one standard error is indicated.*

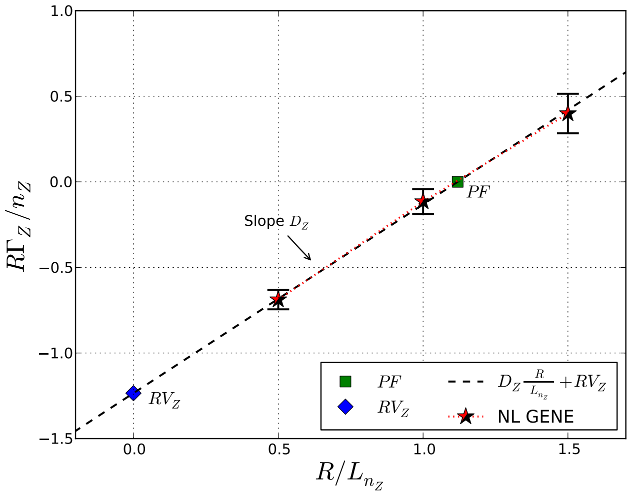

Figure 3.3: *Impurity flux (Γ_Z) dependence on the impurity density gradient (R/L_{n_Z}), illustrating the peaking factor (PF), the diffusivity (D_Z) and pinch (V_Z), and the validity of the linearity assumption of equation (2.16) for trace impurities. Γ_Z is acquired as a time average of the impurity flux; see figure 3.2. D_Z and V_Z are calculated from the data, taking the estimated uncertainty into account. NL GENE simulations with He impurities; parameters as in figure 4.1a. An estimated uncertainty of one standard error is indicated.*

2. the data points are highly correlated.

The first problem can be addressed by various Bayesian schemes [41–43], however, the ordinary variance measure still gives an honest and robust measure of the spread, and – if the process is decidedly unimodal[2] – a measure of the quality of the mean value [44]. This is sufficient for our purposes, since the spread of the time-series are of little interest except as weights in the further post-processing. The second issue can also be dealt with, by seeking an 'effective sample length' s for the data, where $s/N = N_{\text{eff}}$ is the effective number of samples in the time-series. This yields $\sigma \approx \sqrt{\mathrm{Var}[x_i]s/N}$. The quantity s is also referred to as 'statistical inefficiency' and relates to the correlation time, τ, for the time-series as $s = 2\tau/\Delta t$, where Δt is the (average) time-step between data points [45, 46].[3]

Three methods of finding the sample length s have been compared in this work. All three methods give similar results, with typically 10–12 effective samples per $100\,R/c_{\mathrm{s}}$ ($\tau \sim 5\,R/c_{\mathrm{s}}$) for the time-series under consideration. The first two methods use the auto-correlation, $\varPhi_k$, of the time-series as their starting point [45]:

$$\varPhi_k = \frac{\langle \varGamma_{i+k}\varGamma_i \rangle - \langle \varGamma_i \rangle^2}{\langle \varGamma_i^2 \rangle - \langle \varGamma_i \rangle^2}, \tag{3.2}$$

where $\varGamma_i$ is the ith data point, k is the distance in sample space, and $\langle \cdots \rangle$ denotes an average over i. The sample length s can then be calculated from $\varPhi_k$ as [45, 46]:

$$s \approx \sum_{k=-M}^{M} \varPhi_k, \tag{3.3}$$

where $s < M \ll N$. Under the assumption that $\varPhi_k$ decays approximately exponentially with k, the sum in (3.3) can be evaluated explicitly. Assuming the rate of decay with k is slow, the sum can be approximated to good accuracy by finding s from $\varPhi_s = \mathrm{e}^{-2}$. For the time-series considered, this method agrees within a few percent with (3.3), though the simpler method in general gives slightly larger error estimates. This is likely due to the somewhat arbitrary nature of the truncation of the sum in (3.3). This simpler method also lends itself well to automated data-analysis [45].[4]

[2] i.e. the distribution has only one well-defined 'bump'

[3] It should be noted that in the following it is assumed that Δt is approximately constant. If this does not hold, it is a good idea to approximate the data with a first order spline and resample at regular intervals, using e.g. $\Delta t_{\text{new}} \approx 2\,\langle \Delta t \rangle$, before proceeding. For our time-series, however, the difference in the result is negligible.

[4] An even simpler estimate is to only calculate the nearest-neighbour correlation ($\varPhi_1$) and estimate the exponential decay rate from this. By solving for $\varPhi_s = \mathrm{e}^{-2}$, this leads to $s = -2/\ln \varPhi_1$. Though this is a common method, and tempting in its simplicity, this estimate is abysmal for our time-series, giving sample lengths an order of magnitude higher than any of the other methods. This is because the decay for small k is not exponential in our data [42].

The third method is called 'data-blocking'. This method relies on dividing the data into n_B blocks of length M, with $s < M \ll N$. For each block j, the block average $\langle \Gamma \rangle_j$ is calculated, and the sample length can then be estimated from [45, 46]:

$$s = \lim_{M \text{large}} \frac{M \mathrm{Var}\left[\Gamma_{\mathrm{blocks}}\right]}{\mathrm{Var}\left[\Gamma_{\mathrm{all}}\right]}, \tag{3.4}$$

where Γ_{blocks} is the set of n_B block averages, and Γ_{all} is the original data set. For the time-series analysed in this thesis this method has poorer convergence than the other methods. This is because the block lengths needed are too long compared to the total number of samples, which gives poor statistics for $\mathrm{Var}\left[\Gamma_{\mathrm{blocks}}\right]$. The method does, however, yield estimates of the same order of magnitude as the other methods and has therefore been used as an additional 'sanity check' for the acquired results.

3.2.2 Peaking factors

Trace Impurities

The direct method of computing the peaking factor for trace impurities is to compute the average particle flux for different values for the impurity density gradient ($-R\nabla n_Z/n_Z = R/L_{n_Z}$), and fitting the data to equation (2.16). This is illustrated in figure 3.3. The curve fit was performed using the method of least squares, taking the estimated error in the individual data into account [42, 43].[5] The quotient of the obtained diffusion coefficient (D_Z) and convective velocity (RV_Z) then yields the peaking factor (PF), which quantifies the balance of diffusive and convective transport for the impurity species (see section 2.5 for details). The uncertainty estimate obtained from the least squares fit for D_Z and RV_Z can then be propagated to give an error estimate for PF_Z:

$$\sigma_{PF_Z} = \sqrt{\frac{\sigma^2_{D_Z}}{D_Z^2} + \frac{\sigma^2_{RV_Z}}{(RV_Z)^2} - 2\frac{\sigma^2_{D_Z,RV_Z}}{D_Z RV_Z}}, \tag{3.5}$$

where $\sigma^2_{D_Z}$ and $\sigma^2_{V_Z}$ are the estimated variances of the diffusivity and pinch respectively, and $\sigma^2_{D_Z,RV_Z}$ is the covariance of the two [42].

Finally, PF is calculated for several different values of e.g. the impurity charge (Z) in order to obtain a scaling, which can be compared to experiments and other models. Such a scaling is presented in figure 4.1a, where the sample followed in the figures mentioned previously has been highlighted (◯).

Main ions

For main ions equation (2.16) is not linear in R/L_n, wherefore a different approach is needed for finding the main ion peaking factor. As for impurities, the

[5]Since fitting a straight line to two data-points is trivial, ideally at least three simulations should be performed in order to get reliable error estimates for the diffusivity and pinch. In practice, at least for light impurities, the convergence is often good enough for the third measurement to add very little information.

main ion flux is calculated for several values of the density gradient; however, instead of a straight line, a higher (typically second) order polynomial $P(R/L_n)$ was fitted to the data, and the PF taken as the appropriate root of P. The error for PF was approximated by finding the corresponding roots of $P \pm \max[\sigma_\Gamma]$, and using the difference between these roots as a measure of σ_{PF}.

3.2.3 Pinch contributions

Just as the convective velocity can be formally divided into its constituent pinches, the peaking factor can also be decomposed [47–50]:

$$\frac{R\Gamma_Z}{n_Z} = D_Z \left(\frac{R}{L_{n_Z}} + C_T \frac{R}{L_{T_Z}} + C_u \frac{R}{L_{u_Z}} + C_p \right)$$
$$\Longrightarrow PF_Z \equiv -C_T \frac{R}{L_{T_Z}} - C_u \frac{R}{L_{u_Z}} - C_p, \quad (3.6)$$

where the C_T term comes from the thermo-pinch, the C_u term from the roto-pinch, and C_p is referred to as 'pure convection'. Here R/L_{n_Z}, R/L_{T_Z} and R/L_{u_Z} are, respectively, the local scale-lengths of the density, temperature and toroidal rotation profiles for impurity species Z. For trace amounts of impurities, all C_i are constant, independent of the impurity gradients. C_p contains contributions from curvature and parallel compression, and can be formally be written as $C_p = C_{\text{curv}} + C_{\text{comp}} Z/A_Z$. These components can also be found uniquely, however, only if the impurities' charge-to-mass ratios can be changed while artificially constraining impurities' Larmor-radii at their proper values [24, 51].

The contributions to the peaking factor can be found from (3.6) by computing the impurity flux for an appropriate set of orthogonal combinations of gradients and charge-to-mass ratios. Unfortunately, in GENE it is at present neither possible to specify the Larmor-radius, nor the toroidal velocity profile on a species level. Therefore only C_T and C_p are readily accessible, if we – for convenience – define C_p to contain the $C_u u'$ term in the presence of sheared toroidal rotation. One example of parameters is presented in table 3.1. For this set of parameters, the components are computed as in the top-half of table 3.2. The table also gives error estimates for non-linear data [42]. An example of this decomposition is given in figure 4.3.

Since the peaking factor and its components are calculated from ratios of fluxes, they can be calculated even from Γ_i given as quasilinear ratios, without an assumed model for the turbulence. If, on the other hand, either a nonlinear code or a quasilinear model extended with a model for the turbulent fluctuation level is used, one can instead obtain the impurity pinches ($RV_Z = RV_{T,Z} + RV_{p,Z}$) and the diffusivity ($D_Z$) directly, as per the bottom half of table 3.2.

Though this method is very straightforward and fairly transparent, it requires choosing the parameters carefully, and has some additional drawbacks: The method is not designed to use all the information in the data in order to get the best estimates of parameters and uncertainties, and therefore does not lend itself well to decreasing the uncertainty by adding additional data points. This can be remedied by using a more general method, for instance regression analysis or Bayesian inference [42]. An example is given in appendix A, where the method of least squares has been adapted to suit this particular case. For the parameters in table 3.1, the two methods are equivalent.

Table 3.1: *Parameters for test species for which contributions from diffusion, thermopinch and pure convection to the impurity transport can be calculated. Impurities 0–2 are identical, except for the gradients of density and temperature;* exp. *denotes experimental value.*

Species	R/L_{n_Z}	R/L_{T_Z}	$\Gamma_i \propto$
0:	0	0	C_p
1:	1	0	$R/L_{n_Z} + C_p$
2:	0	exp.	$-PF_Z = C_T R/L_{T_Z} + C_p$

Table 3.2: *Calculation of the impurity peaking factor and its components, the impurity pinches and diffusivity, and the their associated error estimates from data obtained using the parameter sets in table 3.1. Here, σ_i denotes the estimated standard error of the impurity density flux data Γ_i, and $R/L_{n_Z} = 1$.*

quantity:	calculation:	error estimate:
$C_{T,Z}\frac{R}{L_{T_Z}}$	$\frac{\Gamma_2-\Gamma_0}{\Gamma_1-\Gamma_0}\frac{R}{L_{n_Z}}$	$\frac{\Gamma_2-\Gamma_0}{\Gamma_1-\Gamma_0}\frac{R}{L_{n_Z}}\sqrt{\frac{\sigma_2^2+\sigma_0^2}{(\Gamma_2-\Gamma_0)^2}+\frac{\sigma_1^2+\sigma_0^2}{(\Gamma_1-\Gamma_0)^2}}$
$C_{p,Z}$	$\frac{\Gamma_0}{\Gamma_1-\Gamma_0}\frac{R}{L_{n_Z}}$	$\frac{\Gamma_0}{\Gamma_1-\Gamma_0}\frac{R}{L_{n_Z}}\sqrt{\frac{\sigma_0^2}{\Gamma_0^2}+\frac{\sigma_1^2+\sigma_0^2}{(\Gamma_1-\Gamma_0)^2}}$
PF_Z	$-C_{T,Z}\frac{R}{L_{T_Z}} - C_{p,Z} = -\frac{\Gamma_2}{\Gamma_1-\Gamma_0}\frac{R}{L_{n_Z}}$	$\frac{\Gamma_2}{\Gamma_1-\Gamma_0}\frac{R}{L_{n_Z}}\sqrt{\frac{\sigma_2^2}{\Gamma_2^2}+\frac{\sigma_1^2+\sigma_0^2}{(\Gamma_1-\Gamma_0)^2}}$
$RV_{T,Z}$	$\frac{R}{n_Z}(\Gamma_2-\Gamma_0)$	$\frac{R}{n_Z}\sqrt{\sigma_2^2+\sigma_0^2}$
$RV_{p,Z}$	$\frac{R}{n_Z}\Gamma_0$	$\frac{R}{n_Z}\sigma_0$
RV_Z	$\frac{R}{n_Z}\Gamma_2$	$\frac{R}{n_Z}\sigma_2$
D_Z	$\frac{R}{n_Z}(\Gamma_1-\Gamma_0)\Big/\frac{R}{L_{n_Z}}$	$\frac{R}{n_Z}\sqrt{\sigma_1^2+\sigma_0^2}$

4

Summary of papers

4.1 Fluid and gyrokinetic simulations of impurity transport at JET

Paper **I** deals with impurity transport due to ion temperature gradient (ITG) mode dominated turbulence in the core plasma region of dedicated impurity injection experiments #67730 and #67732 at JET. The main results are comparisons between experimental results and results from nonlinear and quasilinear gyrokinetic and nonlinear fluid simulations for the impurity peaking factor (see section 2.5) in the form of scalings of the peaking factor (PF) with the impurity charge number Z. The simulations were performed both with one impurity species alone, and with impurities along with 2% C background, which is the common scenario at JET.

A good qualitative agreement between the experimental impurity peaking and both models was obtained, except for Carbon impurities, where the flat or hollow profiles observed in experiments were not reproduced by the numerical simulations. It was observed that the peaking factor increased rapidly for low impurity charge, reaching a saturation for higher values of Z with $2 \lesssim PF \lesssim 3$, which is much lower than neoclassical predictions. Further, the effects of increasing the charge fraction of impurities, of collisions, and of $\boldsymbol{E} \times \boldsymbol{B}$ shearing on the impurity peaking were investigated. The effect of the $\boldsymbol{E} \times \boldsymbol{B}$ shearing was included only as a Dimits shift on the growthrates, neglecting roto-diffusion. All three resulted in lowered peaking factors for the low Z impurities. Scalings with the ion temperature gradient for different species of impurities were also obtained, and also here a good qualitative agreement between the models was observed, though the nonlinear gyrokinetic simulations predicted substantially higher fluctuation levels than the fluid model.

The article was published in Plasma Physics and Controlled Fusion in October 2011 (vol. 53, no. 10, p. 105005).

4.2 Impurity transport in temperature gradient driven turbulence

Rather than comparing with experiments, as in Paper **I**, the main focus in Paper **II** is the comparison of numerical models: nonlinear and quasilinear gyrokinetics, and a computationally efficient nonlinear multi-fluid model. The secondary focus is the comparison of temperature gradient driven TE mode scalings of the impurity peaking factor, with results for the ITG mode similar to those studied in Paper **I**.

Scalings of the impurity peaking factor with the impurity charge number, and with the background temperature and density gradients ($R/L_{T_{i,e}}$ and R/L_{n_e}) were obtained for both modes of turbulence. Nonlinear gyrokinetic scalings with Z and R/L_{T_e} were obtained for the TE mode dominated case.

A falling trend of PF observed for increasing Z in the TE mode case was observed, whereas for the ITG mode the same trend as in Paper **I** was seen, with the peaking factor saturating at higher values of Z for both modes. This is illustrated in in figure 4.1. A theoretical explanation for this difference was found from the signs and Z dependence of the thermodiffusive contribution to the impurity convective velocity, which for TE modes is strictly inward under normal circumstances; see section 2.6.

For all the scalings, the results show a good qualitative agreement between the models. The quasilinear gyrokinetic simulations were observed to overestimate the peaking factor, compared to the nonlinear results. The fluid results were, however, shown to be sensitive to the choice of the parallel mode structure assumed in the simulations, which may hint at an avenue of improvement for the fluid model.

The impurity peaking factor was also compared to the main ion peaking factor as calculated from fluid simulations. The main ion peaking was found to be slightly larger than the corresponding impurity peaking factors.

The work included in this paper builds in part on results presented at the *EPS*, *PDC*, and *RUSA* conferences in 2010; see page vi. It was published in Physics of Plasmas in March 2012 (vol. 19, no. 3, p. 032313).

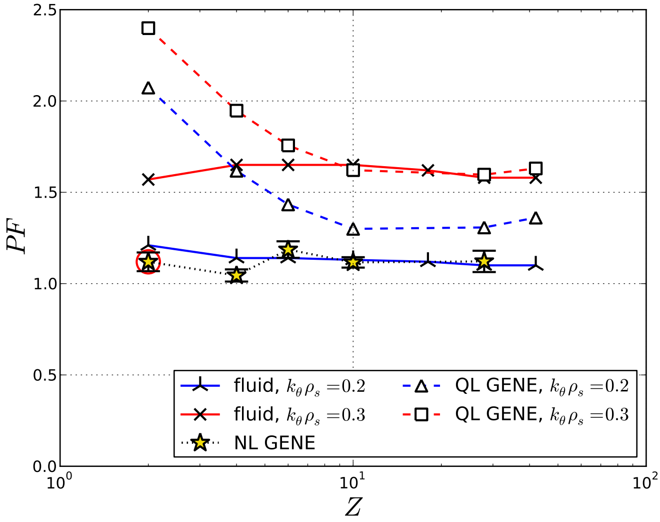

(a) dependence of the peaking factor (PF) on Z for the TE case

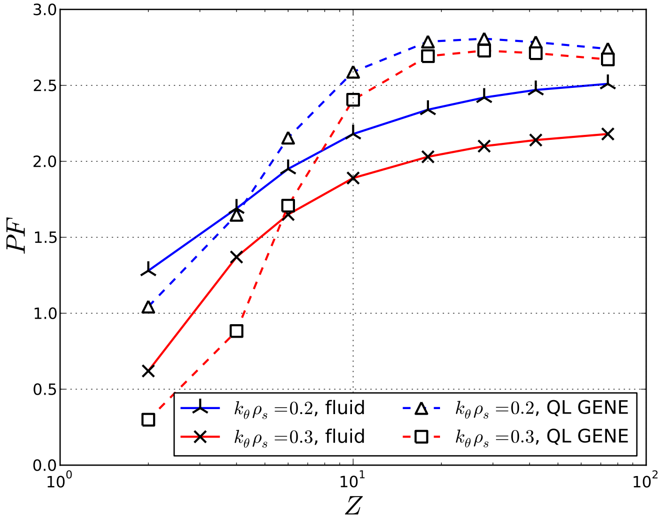

(b) dependence of the peaking factor (PF) on Z for the ITG case

Figure 4.1: *Scalings of the peaking factor (PF) with impurity charge (Z). Parameters are $q = 1.4$, $s = 0.8$, $\epsilon = r/R = 0.143$ in both subfigures, with $R/L_{T_i} = R/L_{T_Z} = 3.0$, $R/L_{T_e} = 7.0$, $R/L_{n_e} = 2.0$ for the TE case (figure 4.1a), and $R/L_{T_i} = R/L_{T_Z} = 7.0$, $R/L_{T_e} = 3.0$, $R/L_{n_e} = 3.0$ for the ITG case (figure 4.1b). The error bars for the NL GENE results in figure 4.1a indicate an estimated error of one standard deviation. The sample for the He impurity acquired from the data illustrated in figure 3.3 and figure 3.2 is highlighted (◯).*

4.3 Particle transport in density gradient driven TE mode turbulence

The work in Paper **III** complements the work in Paper **II** by investigating impurity transport in TE mode turbulence driven by steep background density gradients, as relevant to H-mode physics.

Main ion and impurity transport were both examined, and scalings with Z and R/L_{n_e} obtained from a quasi- and nonlinear gyrokinetic model were compared with results from the fluid model. The scaling with impurity charge was observed to be weak for the parameters considered, and the peaking factor was shown to saturate at values significantly smaller than the driving electron gradient in the steep electron gradient regime. Good qualitative agreements between the models were obtained, and it was observed that, for the TE mode, the quasilinear gyrokinetic simulations usually overestimated PF, whereas the fluid results underestimated it, compared to the nonlinear gyrokinetic results.

The work included in this paper was presented at the *13th International Workshop on H-mode Physics and Transport Barriers* in 2011; see page vi. It was published in Nuclear Fusion in November 2012 (vol. 52, no. 11, p. 114015).

4.4 Effects of the equilibrium model on impurity transport in tokamaks

In Paper **IV** we returned to the JET discharge studied in Paper **I**. The new focus in this study was the effect of additional realism in the simulations on the impurity transport. Of primary interest was the effect of realistic magnetic geometry. It was found that, for the parameters in question, elongation was destabilising, and that the peaking factors were substantially lowered for impurities with high charge number. By comparing diffusivities and pinches between the different cases, it was concluded that the main reason for this was that the pure convection – which is dominated by the curvature pinch – was lowered for the shaped plasma. It was further seen that collisions had a considerable effect on the peaking factors, increasing them for high-charge impurities. This was found to be due to a lower diffusivity for all impurities in case with collisions, consistent with the lower growthrates and fluctuation levels observed. For the lighter impurities, this increase in the peaking factor was offset by a stronger outward thermopinch than in the collisional case, bringing the peaking down to the same level as in the collisionless case. By comparing the transport spectra for these two cases, this difference could be attributed to the (inward) second order term in the thermopinch, which is of less importance for the higher mode frequencies observed in the collisional case. This is illustrated in figure 4.3.

The work was presented at the 2013 EPS, RUSA and WIT conferences. The article was published in Nuclear Fusion in January 2014 (vol. 54, no. 1, p. 013009).

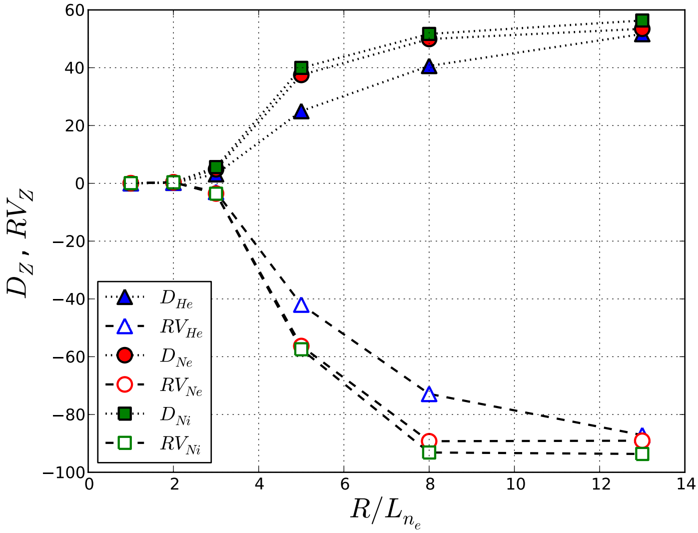

Figure 4.2: *Scalings of the impurity diffusivities (D_Z) and pinches (V_Z) with the background electron density gradient (R/L_{n_e}). As discussed in section 2.5, the impurity peaking factors are calculated from these as $PF_Z = -RV_Z/D_Z$.*

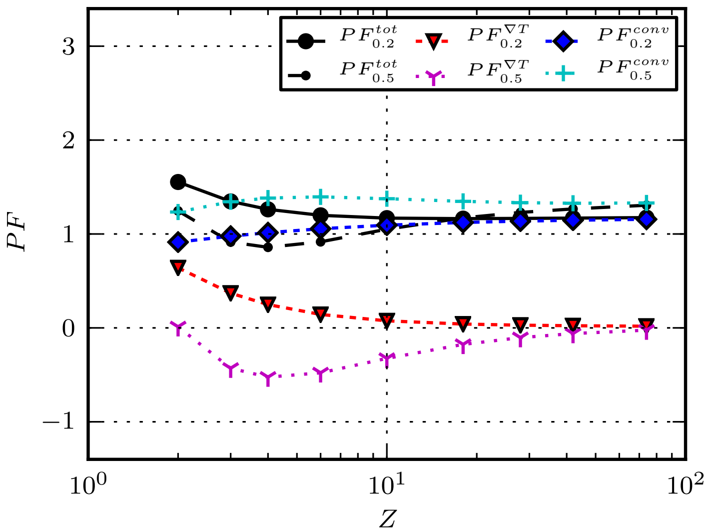

Figure 4.3: *Contributions to the peaking factor ($PF^{tot}_{k_\theta\rho_s}$) from thermodiffusion ($PF^{\nabla T}_{k_\theta\rho_s}$) and pure convection ($PF^{conv}_{k_\theta\rho_s}$) as a function of impurity charge (Z). Results from QL GENE for JET discharge #67730, including effects of shaping ($\kappa = 1.37$, $\delta = 0.044$), 2%C background and collisions.*

4.5 Gyrokinetic modelling of stationary electron and impurity profiles in tokamaks

The final article expands from the field of impurity transport, into selfconsistent treatments of quasi- and nonlinear electron and impurity transport. As a point of departure the parameters from the Cyclone Base Case were used. These are qualitatively similar to the parameters for the ITG mode dominated cases in the previous articles.

It has been show, e.g. in Paper **III**, that the impurity peaking can be sensitive to the background density gradient. Selfconsistent scalings of the electron and impurity peaking factors were therefore calculated for several key plasma parameters, such as magnetic shear, ion–electron temperature ratio, collisionality, safety factor and sheared toroidal rotation. As seen previously for impurities, quasilinear simulations showed stronger peaking than the nonlinear, and also higher sensitivity to the parameters under study. The electron peaking was seen to be most sensitive to collisionality, magnetic shear and ion–electron temperature ratio, making a selfconsistent treatment of the impurity transport important in these cases. The electron peaking was less sensitive to safety factor and sheared toroidal rotation, and also to the driving main ion temperature gradient, which nonetheless showed the expected stiff increase ion thermal transport, as seen in figure 4.4a. The effect of main ion isotope was also studied, and seen to be small, but significant for high collisionalities and ion–electron temperature ratios.

The impurity simulations, using the obtained steady state electron gradients for the background, showed that the simultaneous impurity stationary profiles were consistently less peaked than their electron counterparts. The electron and impurity scalings were mostly qualitatively similar, though less so for impurities with high charge numbers, see figure 4.4b. The impurity scaling with toroidal rotation was strong enough to lead to flux reversal for large toroidal velocities for all impurities, despite the moderate trend seen for the electrons.

Explanations for the impurity scalings were sought from investigating the scaling of thermodiffusive and convective contributions to the impurity peaking factors.

The article is to be submitted to Physics of Plasmas.

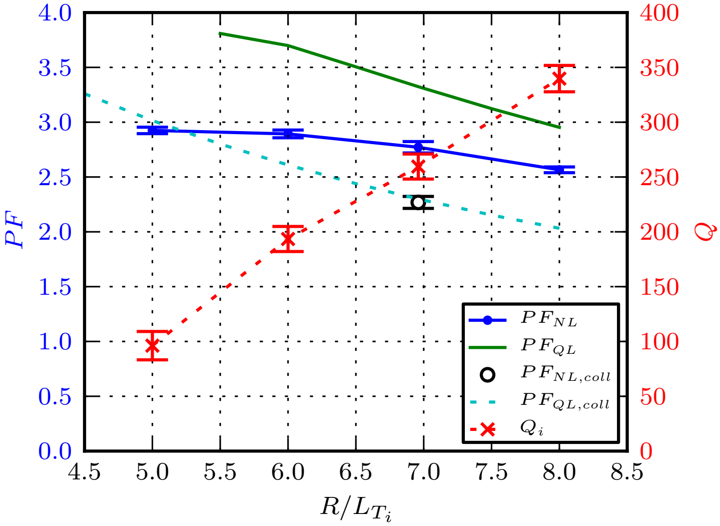

(a) dependence of the electron peaking factor and ion heat flux on ∇T_i; results from NL and QL GENE simulations

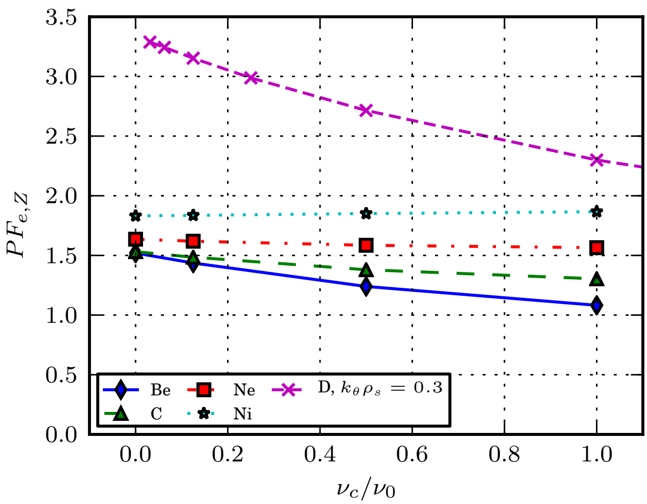

(b) dependence of the electron and impurity peaking factors on collisionality (ν_{ei}); results from QL GENE simulations

Figure 4.4: *Selfconsistent electron and impurity peaking factors, and ion heat flux scalings for the Cyclone Base Case. (*a*) shows stiffness of NL heat flux, while the NL PF_e shows only a moderate scaling. (*b*) shows selfconsistent impurity PF scaling is differs with charge number, and is lower than the corresponding electron peaking.*

Bibliography

[1] W Gibson and B Sterling. *The Difference Engine*. Bantam Books, 1991.

[2] J Wesson. *The Science of JET*. JET Joint Undertaking, 2000. URL http://www.iop.org/Jet/fulltext/JETR99013.pdf.

[3] K S Krane. *Introductory Nuclear Physics*. John Wiley & Sons, Inc., 1988.

[4] A Einstein. Ist die Trägheit eines Körpers von seinem Energieinhalt abhängig? *Annalen der Physik*, 323(13):639–641, 1905.

[5] C Nordling and J Österman. *Physics Handbook*. Studentlitteratur, 6th edition, 1999. “Physics”.

[6] F F Chen. *Introduction to Plasma Physics and Controlled Fusion*, volume Volume 1: Plasma Physics. Plenum Press, 2nd edition, 1984.

[7] J Weiland. *Collective Modes in Inhomogeneous Plasmas*. IoP Publishing, Bristol, UK, 2000.

[8] T Yutani, H Nakamura, M Sugimoto, M Ida, and H Takeuchi. Tritium processing and tritium laboratory in the International Fusion Materials Irradiation Facility (IFMIF). *Fusion Science and Technology*, 41(3P2): 850–853, 2002.

[9] M Pössel. Is the whole the sum of its parts? *Einstein Online*, 4:1003, 2010.

[10] Large Helical Device (LHD). URL http://www.lhd.nifs.ac.jp/en/.

[11] Wendelstein 7-X (W7-X). URL http://www.ipp.mpg.de/ippcms/eng/for/projekte/w7x/.

[12] *“tokamak”*, Merriam-Webster.com, 2011. Merriam–Webster, Inc. URL http://www.merriam-webster.com/dictionary/tokamak. (Dec. 17, 2011).

[13] R D Hazeltine and J D Meiss. *Plasma Confinement*. Dover Publications, 2003.

[14] ITER[1]. URL http://www.iter.org/.

[15] C S Harte, C Suzuki, T Kato, H A Sakaue, D Kato, N Tamura, S Sudo, R D'Arcy, E Sokell, J White, and G O'Sullivan. Tungsten spectra recorded at the LHD and comparison with calculations. *J. Phys. B*, 43 (20):205004, 2010.

[16] Joint European Torus (JET). URL http://www.efda.org/jet/.

[17] G F Matthews, P Edwards, H Greuner, A Loving, H Maier, Ph Martens, V Philipps, V Riccardo, M Rubel, C Ruset, A Scmidt, and E Villedieu. Current status of the JET ITER-like Wall Project. *Phys. Scr.*, 2009 (T138):014030, 2009.

[18] A Loarte, J W Hughes, M L Reinke, J L Terry, and B LaBombard et al. High confinement/high radiated power H-mode experiments in Alcator C-Mod and consequences for International Thermonuclear Experimental Reactor (ITER) $Q_{DT} = 10$ operation. *Phys. Plasmas*, 18(5):056105, 2011.

[19] A Einstein. Über die von der molekularkinetischen Theorie der Wärme geforderte Bewegung von in ruhenden Flüssigkeiten suspendierten Teilchen. *Annalen der Physik*, 323(8):549–560, 1905.

[20] P C Liewer. Measurements of microturbulence in tokamaks and comparisons with theories of turbulence and anomalous transport. *Nucl. Fusion*, 25(5):543, 1985.

[21] C Angioni and A G Peeters. Direction of impurity pinch and auxiliary heating in tokamak plasmas. *Phys. Rev. Lett.*, 96:095003, 2006.

[22] H Nordman, T Fülöp, J Candy, P Strand, and J Weiland. Influence of magnetic shear on impurity transport. *Phys. Plasmas*, 14(5):052303, 2007.

[23] H Nordman, R Singh, T Fülöp, L-G Eriksson, R Dumont, J Anderson, P Kaw, P Strand, M Tokar, and J Weiland. Influence of the radio frequency ponderomotive force on anomalous impurity transport in tokamaks. *Phys. Plasmas*, 15:042316, 2008.

[24] H Nordman, A Skyman, P Strand, C Giroud, F Jenko, F Merz, V Naulin, T Tala, and the JET–EFDA contributors. Fluid and gyrokinetic simulations of impurity transport at JET. *Plasma Phys. Contr. F.*, 53 (10):105005, 2011.

[25] A Hirose, L Zhang, and E Elia. Higher order collisionless ballooning mode in tokamaks. *Phys. Rev. Lett.*, 72(25):3993–3996, 1994.

[26] T M Antonsen and B Lane. Kinetic equations for low frequency instabilities in inhomogeneous plasmas. *Phys. Fluids*, 23(6):1205, 1980.

[1] formerly "International Thermonuclear Experimental Reactor"

[27] E A Frieman and L Chen. Nonlinear gyrokinetic equations for low-frequency electromagnetic waves in general plasma equilibria. *Phys. Fluids*, 25(3):502, 1982.

[28] T S Hahm, W W Lee, and A Brizard. Nonlinear gyrokinetic theory for finite-beta plasmas. *Phys. Fluids*, 31(7):1940, 1988.

[29] A Brizard. Nonlinear gyrokinetic Maxwell–Vlasov equations using magnetic co-ordinates. *J. Plasma Phys.*, 41(3):541, 1989.

[30] F. Jenko and W. Dorland. Nonlinear electromagnetic gyrokinetic simulations of tokamak plasmas. *Plasma Phys. Contr. F.*, 43(12A):A141, 2001.

[31] F Merz. *Gyrokinetic Simulation of Multimode Plasma Turbulence*. Ph.d. thesis (monography), Westfälischen Wilhelms-Universität Münster, 2008.

[32] G Tardini. *Validation of theory based transport models in tokamak plasmas*. Ph.d. thesis (monography), Technishe Univestität München, 2003.

[33] W Arter. Numerical simulation of magnetic fusion plasmas. *Rep. Prog. Phys.*, 58(1):1, 1995.

[34] O G Bakunin. Scaling law and fractality concepts in models of turbulent diffusion. *Plasma Phys. Contr. F.*, 45(10):1909, 2003.

[35] C Bourdelle, X Garbet, F Imbeaux, A Casati, N Dubuit, R Guirlet, and T Parisot. A new gyrokinetic quasilinear transport model applied to particle transport in tokamak plasmas. *Phys. Plasmas*, 14(11):112501, 2007.

[36] C Angioni, Y Camenen, F J Casson, E Fable, R M McDermott, A G Peeters, and J E Rice. Off-diagonal particle and toroidal momentum transport: a survey of experimental, theoretical and modelling aspects. *Nucl. Fusion*, 52(11):114003, 2012.

[37] J Nilsson, M Liljeström, and J Weiland. Fully toroidal fluid model for low-frequency localized modes in magnetized plasmas. *Phys. Fluids B*, 2 (11):2568, 1990.

[38] The GENE code. URL `http://www.ipp.mpg.de/~fsj/gene/`.

[39] T Dannert. *Gyrokinetische Simulation von Plasmaturbulenz mit gefangenen Teilchen und elektromagnetischen Effekten*. Ph.d. thesis (monography), Technischen Universität München, 2005.

[40] T Dannert and F Jenko. Gyrokinetic simulation of collisionless trapped-electron mode turbulence. *Phys. Plasmas*, 12(7):072309, 2005.

[41] D S Sivia. Dealing with duff data. In M Sears, V Nedeljkovic, N E Pendock, and Sibisi S, editors, *Proceedings of the Maximum Entropy Conference*, pages 131–7, Port Elizabeth, South Africa, 1996. NMB printers.

[42] D S Sivia and J Skilling. *Data Analysis, A Bayesian Tutorial*. Oxford University Press, 2nd edition, 2006.

[43] D S Sivia. Data analysis – a dialogue with the data. In P Ciarlini, E Filipe, A B Forbes, F Pavese, C Perruchet, and B Siebert, editors, *Advanced Mathematical and Computational Tools in Metrology VII*, volume 72 of *Series on Advances in Mathematics for Applied Sciences*, pages 108–18. World Scientific Publishing Co., 2006.

[44] M H Quenouille. *Rapid Statistical Calculations*. Charles Griffin & Company Limited, London, UK, 1959.

[45] G Wahnström. *Molecular Dynamics*. Chalmers University of Technology, 2013. Lecture notes.

[46] J M Thijssen. *Computational Physics*. Cambridge University Press, 2nd edition, 2007.

[47] F J Casson, A G Peeters, C Angioni, Y Camenen, W A Hornsby, A P Snodin, and G Szepesi. Gyrokinetic simulations including the centrifugal force in a rotating tokamak plasma. *Phys. Plasmas*, 17(10):102305, 2010.

[48] F J Casson, A G Peeters, C Angioni, Y Camenen, W A Hornsby, A P Snodin, and G Szepesi. Erratum: "gyrokinetic simulations including the centrifugal force in a rotating tokamak plasma". *Phys. Plasmas*, 19(9): 099902, 2012.

[49] F J Casson, R M McDermott, C Angioni, Y Camenen, R Dux, E Fable, R Fischer, B Geiger, P Manas, L Menchero, G Tardini, and the ASDEX Upgrade Team. Validation of gyrokinetic modelling of light impurity transport including rotation in ASDEX Upgrade. *Nucl. Fusion*, 53(6): 063026, 2013.

[50] S S Henderson. Low-Z perturbative impurity transport and microstability analysis on MAST. In *Proceedings of EPS*, 2013.

[51] C Angioni and A G Peeters. Gyrokinetic calculations of diffusive and convective transport of α particles with a slowing-down distribution function. *Phys. Plasmas*, 15(5):052307, 2008.

A

Least squares formulation for the impurity transport

This sections adapts the least squares method for use in finding the diffusion, thermopinch and pure convection for impurity transport. For details on the derivation and the terminology, see e.g. [42]. The most common use for the method of least squares is probably that of finding the coefficients that give the best polynomial fit for the data, for instance a straight line as in section 3.2.2, or a second order polynomial as in section 3.2.2.In this section, however, we are concerned with the coefficients of equation 2.16, which has a linear dependence on two separate parameters: R/L_{n_Z} and R/L_{T_Z}. This situation is very similar to that of finding the coefficients of a second order polynomial, but different enough that it deserves some elucidation. In order to make the following calculations more accessible, we reformulate equation (2.16)

$$\frac{R\Gamma}{n} = D_n\omega_n + D_T\omega_T + RV_p, \tag{A.1}$$

with $D_T\omega_T \equiv RV_T$, $\omega_{n,T} \equiv R/L_{n,T}$,[1] and the Z has been dropped for clarity.

If we assume all data points $Y_k = R\Gamma_k/n$ to be independent and reasonably Gaussian with uncertainty σ_k,[2] then the least squares method can be adopted for finding the optimal D_n, D_T and RV_p, and their respective uncertainties. Equation (A.1) also gives a relation for the kth *ideal datum*:

$$y_k = D_n\omega_{n,k} + D_T\omega_{T,k} + RV_p, \tag{A.2}$$

[1] this is notation is ugly, but useful for its clarity

[2] σ_k relates to that of Γ_k in the same way that Y_k relates to Γ_k: $\sigma_k = R\sigma_{\Gamma,k}/n$

where $\omega_{n,k}$ and $\omega_{T,k}$ are the gradients used when acquiring the data point Y_k, and D_n, D_T and RV_p are the sought quantities. Based on this we define the sum of the *normalised residuals* as

$$\chi^2 = \sum_{k=1}^{N} \left(\frac{y_k - Y_k}{\sigma_k} \right)^2 = \sum_{k=1}^{N} \frac{\left(D_n \omega_{n,k} + D_T \omega_{T,k} + RV_p - Y_k\right)^2}{\sigma_k^2}, \tag{A.3}$$

The derivatives of (A.3) with respect to the parameters are

$$\frac{\partial \chi^2}{\partial D_n} = \sum_{k=1}^{N} \frac{2\left(D_n \omega_{n,k} + D_T \omega_{T,k} + RV_p - Y_k\right)\omega_{n,k}}{\sigma_k^2}, \tag{A.4}$$

$$\frac{\partial \chi^2}{\partial D_T} = \sum_{k=1}^{N} \frac{2\left(D_n \omega_{n,k} + D_T \omega_{T,k} + RV_p - Y_k\right)\omega_{T,k}}{\sigma_k^2}, \tag{A.5}$$

$$\frac{\partial \chi^2}{\partial \left(RV_p\right)} = \sum_{k=1}^{N} \frac{2\left(D_n \omega_{n,k} + D_T \omega_{T,k} + RV_p - Y_k\right)}{\sigma_k^2}, \tag{A.6}$$

which is the same as the components of $\nabla\chi^2$. This system of equations can be written more compactly on matrix form:

$$\nabla\chi^2 = \begin{pmatrix} \alpha & \delta & \epsilon \\ \delta & \beta & \phi \\ \epsilon & \phi & \gamma \end{pmatrix} \begin{pmatrix} D_n \\ D_T \\ RV_p \end{pmatrix} - \begin{pmatrix} p \\ q \\ r \end{pmatrix}, \tag{A.7}$$

where $\alpha = \sum w_k \omega_{n,k}^2$, $\beta = \sum w_k \omega_{T,k}^2$, $\gamma = \sum w_k$, $\delta = \sum w_k \omega_{n,k}\omega_{T,k}$, $\epsilon = \sum w_k \omega_{n,k}$, $\phi = \sum w_k \omega_{T,k}$, $p = \sum w_k \omega_{n,k} Y_k$, $q = \sum w_k \omega_{T,k} Y_k$, $r = \sum w_k Y_k$, and $w_k = 2/\sigma_k^2$.

The best estimate of the parameters are found at the minimum of χ^2, which is found at $\nabla\chi^2 = 0$. This can be found by solving the linear matrix equation for (D_n, D_T, RV_p), which is straight forward, but tedious. Once the matrix inversion has been carried out, however, the covariance matrix for the system is given by

$$\begin{pmatrix} \sigma_{nn}^2 & \sigma_{nT}^2 & \sigma_{nV}^2 \\ \sigma_{nT}^2 & \sigma_{TT}^2 & \sigma_{TV}^2 \\ \sigma_{nV}^2 & \sigma_{TV}^2 & \sigma_{VV}^2 \end{pmatrix} = 2 \begin{pmatrix} \alpha & \delta & \epsilon \\ \delta & \beta & \phi \\ \epsilon & \phi & \gamma \end{pmatrix}^{-1}, \tag{A.8}$$

where the diagonal elements are the variances of the sought parameters.

The procedure above is simple to implement, and can with fair ease be modified to suit any formula which is linear in the sought parameters.

Part II

Appended Papers

"If I model a phenomenon accurately, does that mean I understand it? Or might it be a simple coincidence, or an artifact of the technique? Of course, as an ardent simulationist, I myself put much faith in Engine-modeling. But the doctrine can be questioned, no doubt of it."

Dr E. Mallory [1]

Paper I

Fluid and gyrokinetic simulations of impurity transport at JET

H. Nordman, **A. Skyman**, P. Strand, C. Giroud, F. Jenko, F. Merz, V. Naulin, T. Tala and the JET-EFDA Contributors

Reprint from

Plasma Physics and Controlled Fusion
vol. **53**, *no. 10*, *p. 105005*

doi:10.1088/0741-3335/53/10/105005

http://iopscience.iop.org/0741-3335/53/10/105005

Paper II

Impurity transport in temperature gradient driven turbulence

A. Skyman, H. Nordman, P. Strand

Reprint from

Physics of Plasmas
vol. **19**, *no. 3*, *p. 032313*

doi:10.1063/1.3695014

http://scitation.aip.org/content/aip/journal/pop/19/3/10.1063/1.3695014

Paper III

Particle transport in density gradient driven TE mode turbulence

A. Skyman, H. Nordman, P. I. Strand

Reprint from

Nuclear Fusion
vol. **52**, *no. 11*, *p. 114015*

doi:10.1088/0029-5515/52/11/114015

http://iopscience.iop.org/0029-5515/52/11/114015

Paper IV

Effects of the equilibrium model on impurity transport in tokamaks

A. Skyman, L. Fazendeiro, D. Tegnered, H. Nordman, J. Anderson, P. Strand

Reprint from

Nuclear Fusion
vol. **54**, *no. 1*, *p. 013009*

doi:10.1088/0029-5515/54/1/013009

http://iopscience.iop.org/0029-5515/54/1/013009/

Paper V

Gyrokinetic modelling of stationary electron and impurity profiles in tokamaks

A. Skyman, H. Nordman

Preprint

Physics of Plasmas
(to be submitted)